Scattering characteristics of a metasurface covered metamaterial cylindrical object buried below a flat interface

Saba Rahim

Department of Electronics
Quaid-i-Azam University
Islamabad, Pakistan

2024

Scattering characteristics of a metasurface covered metamaterial cylindrical object buried below a flat interface

by

Saba Rahim

In Partial Fulfillment of the Requirements
for the Degree of
Master of Philosophy

Department of Electronics
Quaid-i-Azam University
Islamabad, Pakistan

March, 2024

CERTIFICATE

Certified that the work contained in this dissertation is carried out by Miss Saba Rahim under my supervision.

Supervisor
(Dr. Muhammad Zeeshan Akbar)
Associate Professor
Department of Electronics,
Quaid-i-Azam University Islamabad,
Pakistan.

Submitted through
Head of Department
(Dr. Qaisar Abbas Naqvi)
Professor
Department of Electronics,
Quaid-i-Azam University, Islamabad,
Pakistan.

To
My beloved parents, brothers and caring friends.

ACKNOWLEDGMENT

In the name of ALLAH, who is the beneficent, the merciful. All praise and glory be to ALLAH, Who created the whole world and keeps signs in it for those who think. This thesis would not be possible without the involvement of multiple entities and I feel great desire to convey my thankfulness to them all. Firstly, an acknowledgment to Almighty ALLAH for his benediction and supervision throughout my entire life-time. Deep faith in ALLAH Almighty made me able to accomplish my objectives in life. Also, peace be upon His last and beloved Prophet, Hazrat MOHAMMAD, who showed us the right path. I am also grateful to my parents and brothers who financially supported me. I would like to acknowledge my supervisors Dr. Muhammad zeeshan Akbar, who guided me on this project. I owe thanks to my friend, Nimra Umar, for helping and directing me in a difficult time with the sheer responsibility. Finally, I would like to pay homage to all my colleagues for kind and favorable cooperation during my study time.

Saba Rahim

ABSTRACT

In this thesis we study scattering characteristics of a metasurface covered metamaterial cylindrical object buried below a flat interface. Spectral plane wave representation of fields has been used to study the interaction between metasurface covered cylinderical object and flat interface. The influences of various lossless metasurface surface reactances upon the normalized scattering width of a metasurface covered metamaterial cylinder have been studied. The considered metamaterials are epsilon negative, mu negative, double negative, epsilon near zero, mu near zero and double near zero.

List of Figures

Table of Contents

Chapter 1

Introduction

1.1 Literature Review

The detection of buried objects has been a problem under consideration mostly in geophysics, archeology, submarine, and mine detection fields. In the recent few decades, researchers have paid huge attention towards the evolution of this important idea in the scientific world, i.e. "buried object detection project". The efforts resulting from this study are useful in detection of hidden land mines, pipes, conduits and other buried intriguing things. The detection process of underground buried objects is not easy as it involves many complications such as clutter existence, less penetration of RF signal into moist soil etc. The complications may also arise due to the nature of an object-surface interface as the surface may be partially or fully rough besides the simplest case, i.e., flat surface interface. Many different techniques have been used for the buried object's detection purpose, depending upon the type of object-surface interface, shape, size, geometry and orientation of the object. Detection of circular cylinders is important as underground gas, water, sewage pipes and electricity, telephone, internet cables are all circular cylinders of great lengths. Wave scattering from the buried objects is one of the efficient methods used for this purpose. Electromagnetic waves scattering from objects buried under a slightly rough surface was studied by [1].

In the recent past, for the detection of buried objects, a remarkably efficient technique, namely "acousto-electromagnetic", was introduced by Lawrence and sarabandi [2]. It involves electromagnetic as well as sound waves. The approach works by monitoring the scattered electromagnetic Doppler spectrum obtained by the objects oscillating at resonance. The incident and scattered sound waves not only account for the object oscillations but also

cause the disturbances in the earth layer above the buried object. In this work, Lawrence and Sarabandi considered the problem of detection of a dielectric cylinder immersed in the dielectric half-space with the existence of a slightly rough surface and obtained the solution using a plane wave representation of the field (PWRF).

Another important detection technique was given by Scott and coworkers [3] where Doppler radar is used along with elastic waves for detection of buried objects via disturbances occurring in surface oscillations [3]. A similar study of the scattering characteristics of electromagnetic waves scattered by cylinders placed above the interface in the case of a flat surface, was done by Borghi et al., [4]. D'Yakonov also gave an analytical proposal for detection of cylinders buried under a flat surface [5]. Ogunade [6] and Budko et al. [7] also worked on this concept and solved the problem by expansion of the eigen function of the total fields. Butler et al. [8] and Xu et al. [9] also contributed to investigation of objects buried under flat surfaces and proposed the numerical solution of a problem by using the method of moment (MoM). Scattering of buried objects under rough surfaces has also been studied using (MoM) by Zhang et al. [10] and Shenawee et al. [11].

Scattering from buried inhomogeneous dielectric objects in the presence of an air-earth interface was studied by Ellis and Peden [12]. They solved the problem by employing a two-dimensional method of moment approach using cylindrical pulse basis by functions and point matching. Butler and Xu worked on scattering by buried dielectric cylinders using integral equation methods [13]. Xu and Ao studied scattering by two-dimensional buried lossy dielectric cylinder using the volume integral equation method [14].

Recently, there is a growing interest in the field of metamaterials. Metamaterials are artificially designed composite materials that can be classified mainly into the six categories, i.e., DPS, DNG, DNZ, ENG, ENZ, MNZ, MNG [15–18]. The description of these metamaterials used in our problem are elaborated below and they are assumed lossless.

1.1.1 Double negative (DNG) metamaterials

Double negative metamaterials have negative permittivity and permiability. Such materials are referred to in the literature as double negative (DNG) media, left-handed media and backward wave media. In this thesis, both the permittivity and the permeability are simultaneously negative and called DNG.

1.1.2 Epsilon negative (ENG) metamaterials

Epsilon negative metamaterials have negative permittivity and positive permeabillity and these types of metamaterials exhibit these characteristics in many plasmas. For example, gold or silver are ENG materials in the infrared and visible spectrum.

1.1.3 Mu negative (MNG) metamaterials

Mu negative metamaterials have positive permittivity and negative permeability. Gyrotropic or gyromagnetic materials are a few examples.

1.1.4 Epsilon near zero and mu near zero (ENG and MNZ) metamaterials

For Epsilon near zero (ENZ) and mu near zero (MNZ) metamaterials, we have near zero electromagnetic parameters, i.e., $\epsilon \approx 0$ for an ENZ and $\mu \approx 0$ for an MNZ.

1.1.5 Double near zero (DNZ) metamaterials

These types of metamaterials have both permittivity and permeability approximately equal to zero, i.e., $\epsilon \approx 0$ and $\mu \approx 0$

Electromagnetic metasurfaces (MSs) are thinner layers of metamaterial that consist of a recurring lattice of sub-wavelength elements. Nowadays, they are highly recommended for microwave and antenna applications [19, 20]. Recently, metasurfaces have been used for the designing of leaky-wave antennas or to direct the propagation path of surface or guided waves. Because of small electrical aspects of the unit cell, metasurfaces may be correctly described in the form of surface impedance, which relates the tangential components of the magnetic and electric fields. For an arbitrary frame unit cell, a precise investigation of the metasurfaces could be done by using the spectral method of moments (MoM) technique [21]. Some specific geometries of metasurfaces that consist of integral elements of squared patches or inductive framework [22] and circular patch [23] have been studied. These structures give absolute and balanced isotropic impedance in the specific limit of homogenization and their applications are limited to specific problems. This limitation is solved by using anisotropic impedance tensor, and it widens the applications of metasurfaces [24, 25],

specifically when interacting with surface wave-based optics of transformation [26, 27]. A common anisotropic metasurface is attained by regularly printing tiny elliptical patches on a buried dielectric slab. The ellipse rotations according to the direction of surface wave traveling may give access to managing the field polarization in circular polarized leaky wave antennas or in transmission optics surface wave-based devices. Mencagli et al. [28] have presented a worthy approach for the specification of metasurfaces having elliptical patches imprinted on a buried dielectric slab. It depends on an analytical modeling of the currents streaming on the patches and gives a concise closed form solution of the surface impedance of the metasurface. An expression of inductance and capacitance at the lower frequency has been included along with the related range of applications. These expressions can also be used for more general cases because they have developed from a broad relationship between the metasurface equivalent network representation and the method of moment technique.

In this thesis, we study the scattering characteristics of a circular metamaterial cylinder covered with metasurface (MS) buried under a flat surface under Transeverse Electric (TE) and Transeverse Magnetic (TM) excitations. The effects of various parameters including permittivity, permeability of metamaterial cylinder and surface reactances of metasurface upon Scattering width (SW) have been studied. By using the tangential and double-sided impedance boundary conditions, unknown scattering coefficients have been found. Mathematical formulation for derivation of electric and magnetic fields in each region is mainly dependent upon the Mie thoery. Finally, the scattering widths are calculated.

Chapter 2

Scattering characteristics of a metasurface covered metamaterial cylindrical object buried below a flat interface

To formulate the problem, a cylinder covered with metasurface of fixed radius a and buried below the flat interface with distance d is considered. The cylinder has electromagnetic properties of $\epsilon_2 = \epsilon_0\epsilon_{r2}$ and $\mu_2 = \mu_0\mu_{r2}$ where ϵ_0 and μ_0 are permittivity and permeability of the free space, respectively. The parameters ϵ_{r2} and μ_{r2} show the relative permittivity and relative permeability of the cylinder material, respectively. The problem is divided into three regions, namely, region 0, region 1, and region 2. Region 0 is the region that is above the interface. Electromagnetic parameters for this region are ϵ_0 and μ_0. The electromagnetic characteristics of this region are k_0 and η_0 where k_0 is the free space wave number and η_0 is the intrinsic impedance of the free space. Here $k_0 = \omega\sqrt{\mu_0\epsilon_0}$ and $\eta_0 = \sqrt{\mu_0/\epsilon_0}$. The region 1 is the medium below the interface with electromagnetic parameters of ϵ_1 and μ_1. The electromagnetic characteristics of this region are described in terms of k_1 and η_1. Here $k_1 = \omega\sqrt{\mu_1\epsilon_1}$ and $\eta_1 = \sqrt{\mu_1/\epsilon_1}$. The region 2 is the region occupied by a material cylinder. This cylinder of material is covered with a metasurface. This metasurface has distributed surface impedance of Z^{TM} and Z^{TE}. The geometry of the problem is shown in Fig. 1.

It is initially considered that there is no flat interface and a metasurface covered cylinder is placed in a background medium with electromagnetic parameters of ϵ_1 and μ_1. This cylinder is normally illuminated by a uniform plane wave which travels in the direction

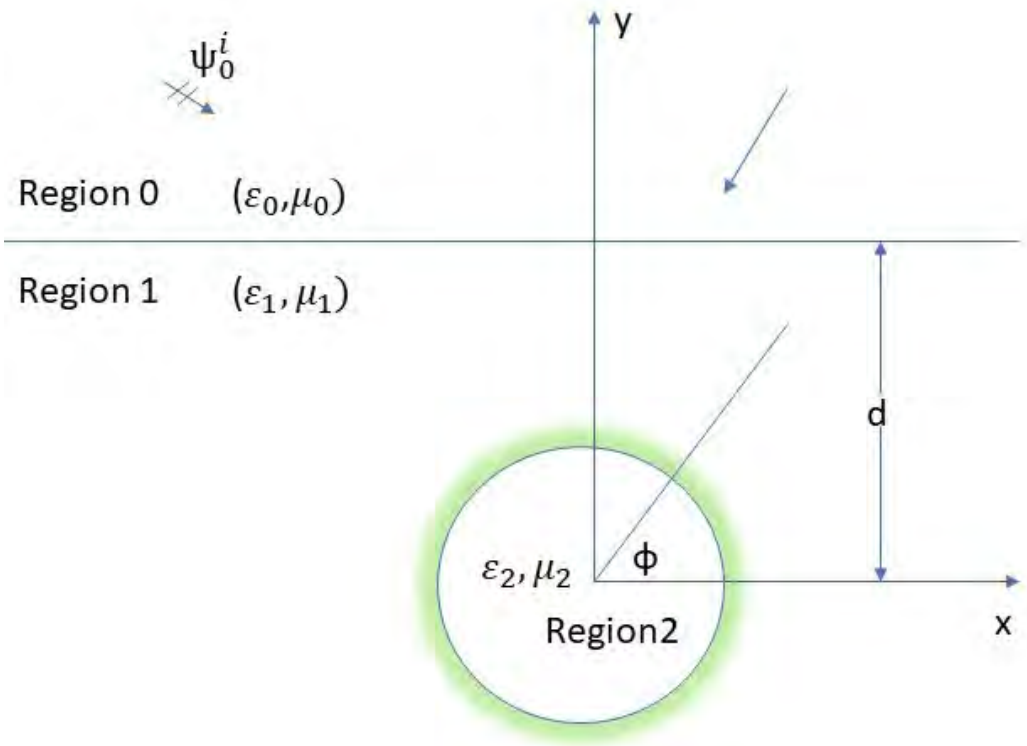

Figure 2.1: The geometrical configuration of a metasurface covered metamaterial cylinder which is buried below a flat interface.

that makes an angle ϕ_o with $+x$–axis. In order to analyze the complete scattering characteristics, both types of incident wave polarizations, i.e., Transverse Magnetic (TM) and Transverse Electric (TE) are considered.

2.1 Transverse Magnetic polarization

For the TM polarization, the z–component of incident electric field E_z^i in region 1 can be written in terms of cylindrical coordinates (ρ,ϕ,z) as below,

$$E_z^i = E_o e^{-jk_1\rho\cos(\phi-\phi_o)} = E_o \sum_{n=-\infty}^{n=+\infty} j^{-n} J_n(k_1\rho) e^{-jn(\phi-\phi_o)} \tag{2.1.1}$$

where E_o is a constant magnitude of electric field and $k_1 = \omega\sqrt{\epsilon_1\mu_1}$ is a wave number of region 1. The function $J_n(\cdot)$ represents an nth order Bessel function of first kind. Likewise, the ϕ–component of the incident magnetic field can be found from the Maxwell's equations as follows,

$$H_\phi^i = -j\frac{E_o}{\eta_1} \sum_{n=-\infty}^{n=+\infty} j^{-n} J_n'(k_1\rho) e^{-jn(\phi-\phi_o)} \tag{2.1.2}$$

where the prime $'$ shows the derivative with respect to the argument. The factor $\eta_1 = \sqrt{\mu_1/\epsilon_1}$ represents the intrinsic impedance of region 1. The z–component of the scattered electric field and the ϕ–component of the magnetic field in region 1 can be expressed as,

$$E_z^s = E_o \sum_{n=-\infty}^{n=+\infty} j^{-n} C_n^{TM} H_n^{(2)}(k_1\rho) e^{-jn(\phi-\phi_o)} \tag{2.1.3}$$

$$H_\phi^s = -j\frac{E_o}{\eta_1} \sum_{n=-\infty}^{n=+\infty} j^{-n} C_n^{TM} H_n^{(2)'}(k_1\rho) e^{-jn(\phi-\phi_o)} \tag{2.1.4}$$

where C_n^{TM} is the unknown scattering coefficient and needed to be determined. $H_n^{(2)}(\cdot)$ is the nth order Hankel function of second kind and represents an outward traveling wave solution. It is well known that the electric field inside the cylinder at $\rho = 0$ must be finite, thus the electric field inside the cylinder can be expressed in terms of only nth order Bessel function of first kind. The electric filed E_z^2 and magnetic field H_ϕ^2 in the region 2 can be written as,

$$E_z^2 = E_o \sum_{n=-\infty}^{n=+\infty} j^{-n} A_n J_n(k_2\rho) e^{-jn(\phi-\phi_o)} \tag{2.1.5}$$

$$H_{\phi}^{2} = -j\frac{E_o}{\eta_2}\sum_{n=-\infty}^{n=+\infty} j^{-n} A_n J_n^{'}(k_2\rho) e^{-jn(\phi-\phi_o)} \tag{2.1.6}$$

where $k_2 = \omega\sqrt{\epsilon_2\mu_2}$ is the wave number of region 2 and $\eta_2 = \sqrt{\mu_2/\epsilon_2}$ is the intrinsic impedance of the material of the cylinder. The unknown coefficients A_n and C_n^{TM} can be found by applying the tangential boundary conditions which states that the tangential electric and magnetic fields must be continuous at $\rho = a$. These boundary conditions can be written as follows,

$$E_z^2 = E_z^i + E_z^s \tag{2.1.7}$$

$$E_z^2 = Z^{TM}[H_{\phi}^1 + H_{\phi}^s - H_{\phi}^1] \tag{2.1.8}$$

By substituting the respective fields in the above two boundary conditions, we obtain two equations as below,

$$J_n(k_1a) = A_n J_n(k_2a) + C_n^{TM} H_n^{(2)}(k_1a) \tag{2.1.9}$$

$$J_n(k_1a) = Z^{TM}[A_n J_n'(k_2a) + C_n^{TM} H_n'^{(2)}(k_1a) - J_n'(k_1a)] \tag{2.1.10}$$

The unknown coefficients C_n^{TM} and A_n can be found by solving Eqs. (2.1.9)–(2.1.10). Thus, unknown coefficient C_n^{TM} which is of an interest for the scattered electric field can be written as,

$$C_n^{TM} = \frac{jJ_n(x_1)J_n(x_2) + Z^{TM}[(\frac{1}{\eta_2})J_n(x_1)J_n'(x_2) - (\frac{1}{\eta_1})J_n(x_2)J_n'(x_1)]}{-jJ_n(x_2)H_n^{(2)}(x_1) + Z^{TM}[(\frac{1}{\eta_1})J_n(x_2)H_n^{(2)}(x_1) - (\frac{1}{\eta_2})J_n'(x_2)H_n^2(x_1)]} \tag{2.1.11}$$

where $x_1 = k_1a$ and $x_2 = k_2a$. It can be shown that if Z_{TM}=0 and $k_2 = k_1$ then this cylinder corresponds to a PEC cylinder and C_n^{TM} becomes same as that of PEC cylinder which is given as,

$$C_n^{TM} = \frac{-J_n(k_1a)}{H_n^{(2)}(k_1a)} \tag{2.1.12}$$

2.2 Transverse Electric polarization

In case of Transverse Electric (TE) polarization, the incident electric field E_{ϕ}^i and incident magnetic field H_z^i are given as,

$$E_{\phi}^i = \eta_1 H_o \sum_{n=-\infty}^{n=+\infty} j^{-n-1} J_n^{'}(k_1\rho) e^{-jn(\phi-\phi_o)} \tag{2.2.1}$$

$$H_z^i = H_o \sum_{n=-\infty}^{n=+\infty} j^{-n} J_n(k_1\rho) e^{-jn(\phi-\phi_o)} \tag{2.2.2}$$

where H_o is a constant magnitude of magnetic field. The z–component of the scattered magnetic field and the ϕ–component of the scattered electric field can be written as,

$$H_z^s = H_o \sum_{n=-\infty}^{n=+\infty} j^{-n} C_n^{TE} H_n^{(2)}(k_1\rho) e^{-jn(\phi-\phi_o)} \tag{2.2.3}$$

$$E_\phi^s = \eta_1 H_o \sum_{n=-\infty}^{n=+\infty} j^{-n-1} C_n^{TE} H_n^{(2)'}(k_1\rho) e^{-jn(\phi-\phi_o)} \tag{2.2.4}$$

where C_n^{TE} is the unknown scattering coefficient and needed to be determined. Likewise, the magnetic filed H_z^2 and electric field E_ϕ^2 in the region 2 can be written as,

$$H_z^1 = H_o \sum_{n=-\infty}^{n=+\infty} j^{-n} B_n J_n(k_2\rho) e^{-jn(\phi-\phi_o)} \tag{2.2.5}$$

$$E_\phi^1 = \eta_2 H_o \sum_{n=-\infty}^{n=+\infty} j^{-n-1} B_n J_n'(k_2\rho) e^{-jn(\phi-\phi_o)} \tag{2.2.6}$$

The unknown coefficients B_n and C_n^{TE} can be found by applying the following boundary conditions,

$$E_\phi^2 = E_\phi^i + E_\phi^s \tag{2.2.7}$$

$$E_\phi^2 = -Z^{TE}[H_z^i + H_z^s - H_z^1] \tag{2.2.8}$$

By substituting the required electric and magnetic field components in the above two boundary conditions, we obtain two equations as below,

$$J_n'(k_1 a) = B_n J_n(k_2 a) + C_n^{TM} H_n'(k_1 a) \tag{2.2.9}$$

$$J_n'(k_1 a) = -Z^{TM} B_n J_n(k_2 a) - Z^{TM} C_n^{TM} H_n(k_1 a) + Z^{TM} J_n(k_1 a) \tag{2.2.10}$$

By solving Eqs. (2.2.9)–(2.2.10) simultaneously, the unknown scattering coefficient C_n^{TE} can be found and is given below.

$$C_n^{TE} = \frac{j J_n'(x_1) J_n'(x_2) + Z^{TE}[(\frac{1}{\eta_1}) J_n(x_1) J_n'(x_2) - (\frac{1}{\eta_2}) J_n(x_2) J_n'(x_1)]}{-j J_n'(x_2) H_n'^{(2)}(x_1) + Z^{TE}[(\frac{1}{\eta_2}) J_n(x_2) H_n'^{(2)}(x_1) - (\frac{1}{\eta_1}) J_n'(x_2) H_n^2(x_1)]} \tag{2.2.11}$$

In case of PEC cylinder, we have Z^{TE}=0 and $k_2 = k_1$, thus the scattering coefficient C_n^{TE} becomes as,

$$C_n^{TE} = \frac{-J_n'(k_1 a)}{\eta_0 H_n'(k_1 a)} \tag{2.2.12}$$

which is expected.

2.3 Scattering properties of a metasurface covered cylinder placed below a flat interface

In this case, the geometry given in Figure 1 is considered. The spectral representation of the fields will be employed in this part to solve the scattered field in Region 1. The solution will be produced by summing the successive scattered fields from the flat surface and the cylinder. Analytical solutions for the scattering of a plane wave from a flat interface and the scattering of a plane wave from a cylinder are known. By using general formulations for the reflected, transmitted, and scattered fields, both TE and TM polarization will be treated simultaneously.

It is possible to obtain the reflected and transmitted fields due to an interface when a metasurface coated cylinder is present. For this case, the incident field is expressed as,

$$\psi_0^i = e^{-j(\gamma_x^i x - \gamma_{0y}^i y)} \tag{2.3.1}$$

where ψ_0^i=E_z^i or H_z^i and γ_{0y}^i=$\sqrt{\gamma_0^2 - (\gamma_x^i)^2}$. The first order reflected field from the boundary can be written as,

$$\psi_0^r = R_{01}(\gamma_x^i) e^{j2\gamma_{0y}^i d} e^{-j(\gamma_x^i x + \gamma^i{}_{0y} y)} \tag{2.3.2}$$

where $R_{01}(\gamma_x^i)$ is the reflection coefficient and given by,

$$R_{01}(\gamma_x^i) = \frac{\gamma_{0y}^i - \gamma_{1y}^i}{\gamma_{0y}^i + \gamma_{1y}^i} \tag{2.3.3}$$

$$\gamma_{1y}^i = \sqrt{\gamma_1^2 - (\gamma_x^i)^2} \tag{2.3.4}$$

The field transmitted into Region 1 can be written as,

$$\psi_0^t = T_{01}(\gamma_x^i) e^{j(\gamma_{0y}^i - \gamma_{1y}^i)d} e^{-j(\gamma_x^i x - \gamma_{1y}^i y)} \tag{2.3.5}$$

where $T_{01}(\gamma_x^i)$ is the transmission coefficient and given by,

$$T_{01}(\gamma_x^i) = \frac{2\gamma_{0y}^i}{\gamma_{0y}^i + \gamma_{1y}^i} \tag{2.3.6}$$

The initial scattered field from the metasurface covered cylinder is given as,

$$\psi_1 = \sum_{n=-\infty}^{\infty} j^{-n} C_n^{TM} H_n^{(2)}(\gamma_1 \rho) e^{jn(\phi-\phi_i)} \tag{2.3.7}$$

The scattered field from the buried cylinder can be written as,

$$\psi_1^1 = \sum_{n=-\infty}^{\infty} j^{-n} C_n^{TM} H_n^{(2)}(\gamma_1 \rho) e^{jn\phi} C_n^{(1)} \tag{2.3.8}$$

$$C_n^{(1)} = T_{01}(\gamma_x^i) e^{j(\gamma_{0y}^i - \gamma_{1y}^i)d} e^{-jn\tan^{-1}(-\gamma_{1y}^i/\gamma_x^i)} \tag{2.3.9}$$

The Eq. (2.3.8) is the scattered field due to the first interaction of buried cylinder. Using the integral representation of $H_n^{(2)}(\gamma_1\rho)\exp^{jn\phi}$ in Eq. (2.3.8), the initial scattered field can be written as,

$$\psi_1^{(1)} = \frac{1}{\pi} \int_{-\infty}^{\infty} \frac{e^{-j(\gamma_x x + \gamma_{1y} y)}}{\gamma_{1y}} \sum_{n=-\infty}^{\infty} C_n^{TM} [C_n^{(1)}] e^{jn\tan^{-1}(\gamma_{1y}/\gamma_x)} d\gamma_x \tag{2.3.10}$$

This field is seen to be the linear combination of plane waves propagating in the $+y$ direction. Based upon this field, the downward reflected field from the flat interface can be written as,

$$\hat{\psi}_1^{(1)} = \frac{1}{\pi} \int_{\gamma_x} \frac{1}{\gamma_{1y}} \sum_{n=-\infty}^{\infty} C_n^{TM} [C_n^{(1)}] e^{jn\tan^{-1}(\gamma_{1y}/\gamma_x)} R_{10}(\gamma_x) e^{-2j\gamma_{1y}d} e^{-j(\gamma_x x - \gamma_{1y} y)} d\gamma_x \tag{2.3.11}$$

This downward reflected field interacts with the metasurface covered cylinder and causes scattering. Using the similar steps as previously, the second order scattered field is given by,

$$\psi_1^{(2)} = \sum_{n=-\infty}^{\infty} j^{-n} C_n^{TM} H_n^{(2)}(\gamma_1 \rho) e^{jn\phi} \frac{1}{\pi} \sum_{m=-\infty}^{\infty} (C_m^{(1)})(I_{m,n}^u) \tag{2.3.12}$$

where

$$I_{m,n}^u = \int_{\gamma_x} \frac{1}{\gamma_{1y}} R_{10}(\gamma_x) e^{-2j\gamma_{1y}d} e^{jm\tan^{-1}(\gamma_{1y}/\gamma_x)} e^{-jn\tan^{-1}(-\gamma_{1y}/\gamma_x)} d\gamma_x \tag{2.3.13}$$

These above Eqs. (2.3.12)–(2.3.13) can be further written in the simplest form as below,

$$\psi_1^{(2)} = \sum_{n=-\infty}^{\infty} j^{-n} C_n^{TM} H_n^{(2)}(\gamma_1 \rho) e^{jn\phi} C_n^{(2)} \tag{2.3.14}$$

$$C_n^{(2)} = \frac{1}{\pi} \sum_{m=-\infty}^{\infty} C_m^{TM} C_m^{(1)} I_{m,n}^u \tag{2.3.15}$$

Likewise, extending this approach, we can find the qth order scattered field in region 1. This field is given below,

$$\psi_1^{(q)} = \sum_{n=-\infty}^{\infty} j^{-n} C_n^{TM} H_n^{(2)}(\gamma_1 \rho) e^{jn\phi} C_n^{(q)} \tag{2.3.16}$$

$$C_n^{(q)} = \frac{1}{\pi} \sum_{m=-\infty}^{\infty} C_m^{TM} C_m^{(q-1)} I_{m,n}^u \tag{2.3.17}$$

Finally, the total scattered field in region 1 will be calculated by adding contributions of all the scattered fields and are given as,

$$\psi_1 = \sum_{q=1}^{\infty} \psi_1^{(q)} \tag{2.3.18}$$

$$\psi_1 = \sum_{q=1}^{\infty} \sum_{n=-\infty}^{\infty} j^{-n} C_n^{TM} H_n^{(2)}(\gamma_1 \rho) e^{jn\phi} C_n^{(q)} \tag{2.3.19}$$

$$\psi_1 = \sum_{n=-\infty}^{\infty} j^{-n} C_n^{TM} H_n^{(2)}(\gamma_1 \rho) e^{jn\phi} C_n \tag{2.3.20}$$

$$C_n = \sum_{q=1}^{\infty} C_n^{(q)} \tag{2.3.21}$$

where C_n defines all the multiple interactions between the metasurface cylinder and flat interface.

$$C_n = C_n^{(1)} + \sum_{q=1}^{\infty} C_n^{(q+1)} \tag{2.3.22}$$

$$C_n = C_n^{(1)} + \sum_{q=1}^{\infty} \frac{1}{\pi} \sum_{m=-\infty}^{\infty} C_m^{TM} C_m^{(q)} I_{m,n}^u \tag{2.3.23}$$

$$C_n = C_n^{(1)} + \frac{1}{\pi}\sum_{m=-\infty}^{\infty} C_m^{TM} C_m I_{m,n}^{u} \tag{2.3.24}$$

At this stage, it is desired to find the scattered field in region 0. For this, the scattered field in region 1 is first expanded into spectral form and using the integral expansion of $H_n^{(2)}(\gamma_1\rho)\exp^{jn\phi}$, the scattered field becomes,

$$\psi_1 = \frac{1}{\pi}\int_{\gamma_x} \frac{1}{\gamma_{1y}} e^{-j(\gamma_x x+\gamma_{1y} y)} \sum_{n=-\infty}^{\infty} C_n^{TM} C_n e^{jn\tan^-1(\gamma_{1y}/\gamma_x)} d\gamma_x \tag{2.3.25}$$

Thus, the scattered field in region 0 becomes,

$$\psi_0^s = \frac{1}{\pi}\sum_{n=-\infty}^{\infty} C_n^{TM} C_n (I_n^{tu}) \tag{2.3.26}$$

where

$$I_n^{tu} = \int_{\gamma_x} \frac{1}{\gamma_{1y}} T_{10}(\gamma_x) e^{jn\tan^{-1}(\gamma_{1y}/\gamma_x)} e^{j(\gamma_{0y}-\gamma_{1y})d} e^{-j(\gamma_x x+\gamma_{0y} y)} d\gamma_x \tag{2.3.27}$$

The total scattered field in the region 0 can be made known provided that if the integral I_n^{tu} is known. This integral I_n^{tu} can be solved using the saddle point integration method. After applying saddle point integration method to the integral I_n^{tu}, the total scattered field can be written as,

$$\psi_0^s = \frac{1}{\pi}\sum_{-\infty}^{\infty} C_n^{TM} C_n I_n^{tu} \tag{2.3.28}$$

$$I_n^{tu} \sim \sqrt{\frac{2\pi}{\gamma_0\rho}} e^{-j\gamma_0\rho - j\frac{\pi}{n}} 2e^{jn\tan^{-1}\left(\frac{\sqrt{\gamma_1^2-\gamma_0^2\cos^2\phi}}{\gamma_0\cos\phi}\right)} \frac{e^{j(\gamma_0\sin\phi-\sqrt{\gamma_1^2-\gamma_0^2\cos^2\phi})d}}{\sqrt{\gamma_1^2-\gamma_0^2\cos^2\phi}+\gamma_0\sin\phi}(-\gamma_0\sin\phi) \tag{2.3.29}$$

We are interested in the far zone region and want to find the scattering width of a cylinder covered with a metasurface. The scattering width SW is defined as given below,

$$\sigma = \lim_{\rho\to\infty} 2\pi\rho \frac{|\ \psi_0^s\ |^2}{|\ \psi_0^i\ |^2} \tag{2.3.30}$$

Now by substituting Eq. (2.3.1) and Eqs. (2.3.28)–(2.3.29) in Eq. (2.3.30), we obtain,

$$\sigma = \frac{4}{k_0}\Big|\sum_{n=-\infty}^{\infty} C_n^{TM} C_n F(\phi)\Big|^2 \tag{2.3.31}$$

Often, it is desired to express SW in unitless manner, therefore, we define normalized SW as $\sigma_n = \sigma/\lambda_0$ which is given below

$$\frac{\sigma}{\lambda_0} = \frac{2}{\pi}\Big| \sum_{n=-\infty}^{\infty} C_n^{TM} C_n F(\phi)\Big|^2 \tag{2.3.32}$$

$$F(\phi) = \frac{-2e^{jn\tan^{-1}\left(\frac{\sqrt{\gamma_1^2-\gamma_0^2\cos^2\phi}}{\gamma_0\cos\phi}\right)}}{\sqrt{\gamma_1^2-\gamma_0^2\cos^2\phi}+\gamma_0\sin\phi}(\gamma_0\sin\phi)e^{j\left(\gamma_0\sin\phi-\sqrt{\gamma_1^2-\gamma_0^2\cos^2\phi}\right)d} \tag{2.3.33}$$

Likewise, using the similar steps, the normalized SW for TE mode can be found. It should be noted that for numerical results, we have used normalized SW, i.e., $\sigma_n = \frac{\sigma}{\lambda_0}$.

Chapter 3

Numerical Results and Discussion

For the numerical results, it is assumed that metasurfce has surface impedance of $Z^{TM} = j\chi_m$ and $Z^{TE} = j\chi_e$. Here χ_m and χ_e represent the surface reactance of a metasurface and they can have positive or negative values. For all the figures, $\lambda_o = 0.1$ m, depth of cylinder is $d = 1.5\lambda_o$ and radius of cylinder is $a = 0.15\lambda_o$. It is clear from figure 3.1 that for TM polarization, the scattering width is relatively large for the PEC cylinder as compared to dielectric and magnetic cylinders. Moreover, metasurface coating is not considered for these figures. Similar behavior is noted for the TE polarization and shown in Fig 3.2.

In figures 3.3 to 3.6, the influence of surface impedance $Z^{TM} = j\chi_m$ upon scattering width of a metasurface covered ENG cylinder has been shown. In this case, both types of incident polarizations have been considered. For completeness, these scattering widths are also compared with the scattering width of an ENG cylinder without metasurface. In case of TE polarization, it is sen from Fig. 3.4 that metasurfaces having $\chi_e = 0.1k\Omega$ and $1k\Omega$ can be used to decrease the SW as compared respective SW of an ENG cylinder without metasurface. For TM polarization, it is observed that metasurfaces having χ_m = -0.01$k\Omega$, -0.1$k\Omega$ and -1$k\Omega$, the scattering width can be enhanced as compared to scattering width of ENG cylinder without metasurface.

In figures 3.7 to 3.10, the effects of surface impedance $Z^{TM} = j\chi_m$ upon scattering width of a metasurface covered MNG cylinder has been shown. These scattering widths of metasurafce covered MNG cylinder have also been compared with the scattering width of an MNG cylinder without metasurface. In case of TM polarization for $45° \leq \phi \leq 180°$, the metasurfaces having χ_m = -0.01$k\Omega$, -0.1$k\Omega$ and -1$k\Omega$ can be used to enhance the scattering width as compared to scattering width of MNG cylinder without metasurface. Likewise, for TE polarization, it is found that scattering widths of MS covered MNG cylinders and

MNG cylinder without MS are almost same.

The figures 3.11–3.14 deal with the effects of surface impedance $Z^{TM} = j\chi_m$ and $Z^{TE} = j\chi_e$ upon scattering width of a metasurface covered DNG cylinder have been shown for both types of incident polarization. Also, these scattering widths have been compared with the scattering width of a DNG cylinder without metasurface. For a DNG cylinder without metasurface, the scattering width has maximum value around $\phi = 110^o$ whereas for DNG covered cylinders having considered values of χ_m, the scattering widths are relatively small at $\phi = 110^o$. Similar behavior is also observed for the TE polarization in Fig. 3.12. In figures 3.13–3.14, the effects of negative values of χ_m and χ_e upon the scattering widths of MS covered DNG cylinder haven been shown. These SWs are also compared with the SW of a DNG cylinder without MS. It is clear from Fig. 3.14 that the scattering width of MS covered DNG cylinder increases for $90^\circ \leq \phi \leq 180^\circ$ having χ_e = -1kΩ as compared to respective SW of a DNG cylinder without MS.

In figures 3.15–3.18, the effects of metasurface reactance χe, χm upon the normalized scattering width of a metasurface covered ENZ cylinder buried below a flat interface have been shown. For completeness, these scattering widths are also compared with the SW of an ENZ cylinder without metasurface. For these figures, both types of incident polarization have been considered. It is observed that the behavior of scattering width is quite different for the ENZ cylinders as compared to the cylinder. Similar trend in figure 3.16 is noted when TE polarization incidence is considered. An important result is observed for a MS covered ENZ cylinder having χ_m = -0.1kΩ which states that the scattering width become maximum at $\phi = 30^o$ and it decreases gradually and become minimum at $\phi = 100^o$. This is clear from Fig. 3.17.

In figures 3.19–3.22, the influence of metasurface reactance χe, χm upon the normalized scattering width of a metasurface covered MNZ cylinder buried below a flat interface have been shown. For completeness, these scattering widths are also compared with buried MNZ cylinder without metasurface. In this case, we have assumed χ_e, $\chi_m = \pm 0.01k\Omega$, $\pm 0.1k\Omega$ and $\pm 1k\Omega$ for both types of incident polarization. It is clear from Fig. 3.20 that metasurfaces with $\chi_e = 0.01k\Omega$ and $0.1k\Omega$, there exists a significant enhancement in SW as compared to SW of an MNZ cylinder without MS for TE polarization.

The figures 3.23–3.26 deal with the influence of metasurface reactance χ_e, χ_m upon the normalized scattering width of a metasurface covered DNZ cylinder buried below a flat interface for various values of χ_e and χ_m. For this, both types of incident polarizations have been considered. These scattering widths are also compared with the DNZ cylinder without metasurface. It is clear from Fig. 3.24 that for $90^\circ \leq \phi \leq 180^\circ$, the scattering widths of MS covered DNZ cylinder having $\chi_e = 0.01k\Omega$, $0.1k\Omega$ and $1k\Omega$ are almost same for TE polarization. In case of TM polarization, it is observed from Fig. 3.25 that considered

capacitive metasurfaces can be used to enhance the overall SWs as compared to SW of a DNZ cylinder without MS.

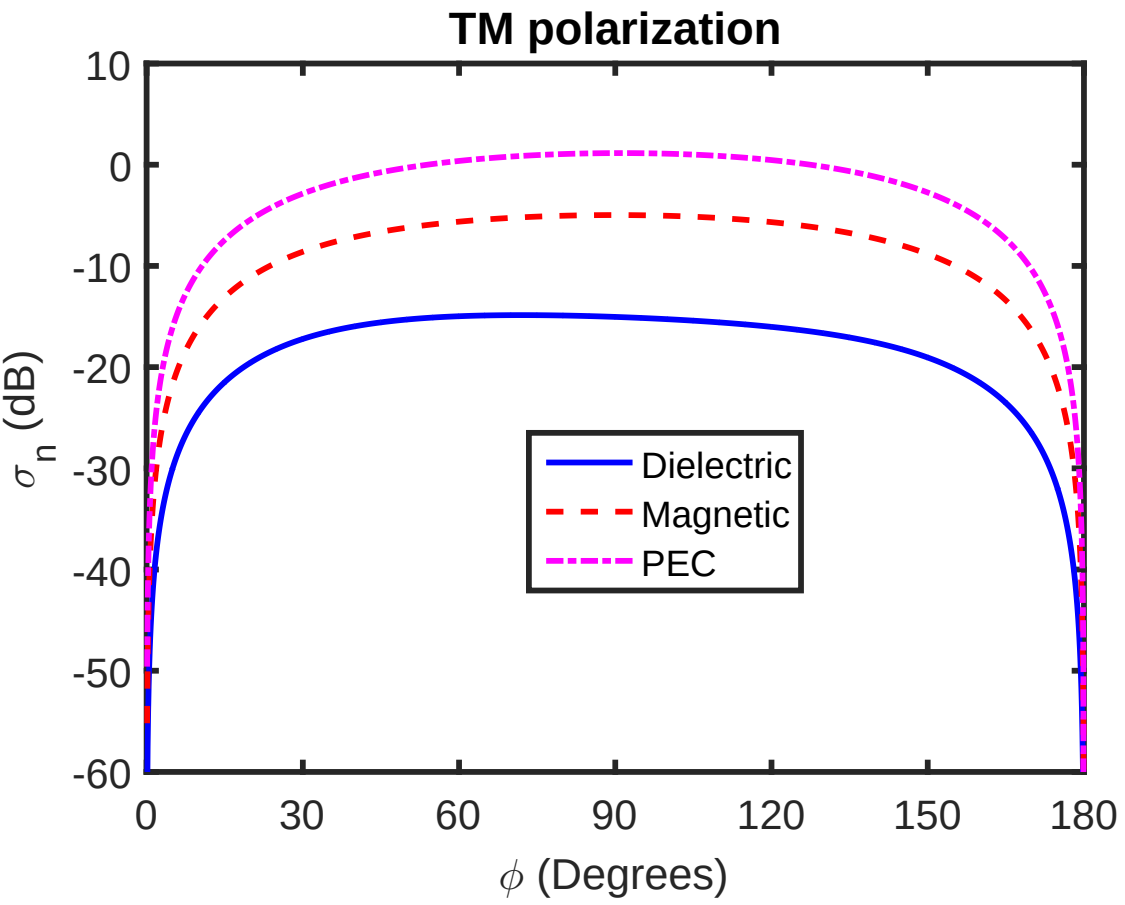

Figure 3.1: Normalized scattering widths of buried dielectric, magnetic and perfectly electric conducting (PEC) cylinders under TM polarization. For dielectric cylinder,we have $\epsilon_r = 2.25$, $\mu_r = 1$ and for magnetic cylinder $\epsilon_r = 1$, $\mu_r = 2.25$. Here these cylinders are not covered with metasurface.

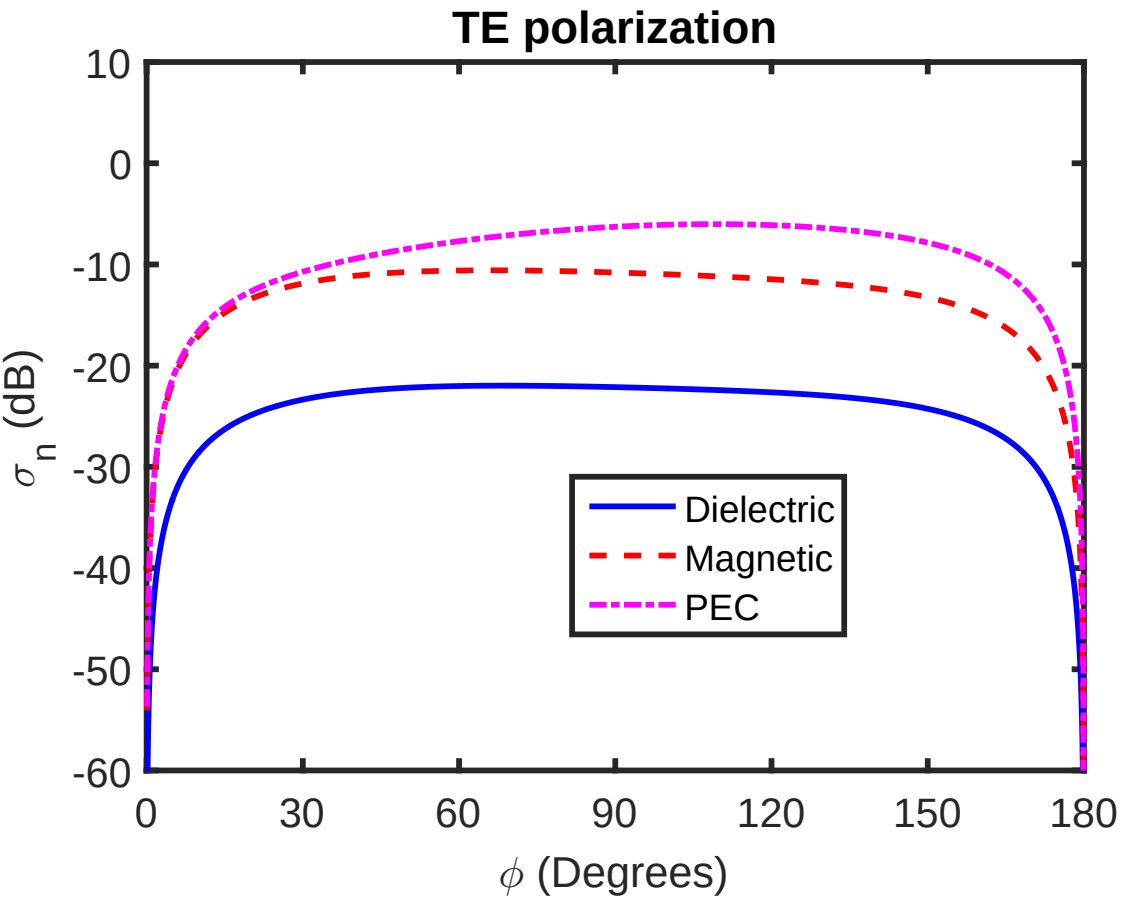

Figure 3.2: Normalized scattering widths of buried dielectric, magnetic and perfectly electric conducting (PEC) cylinders under TE polarization.

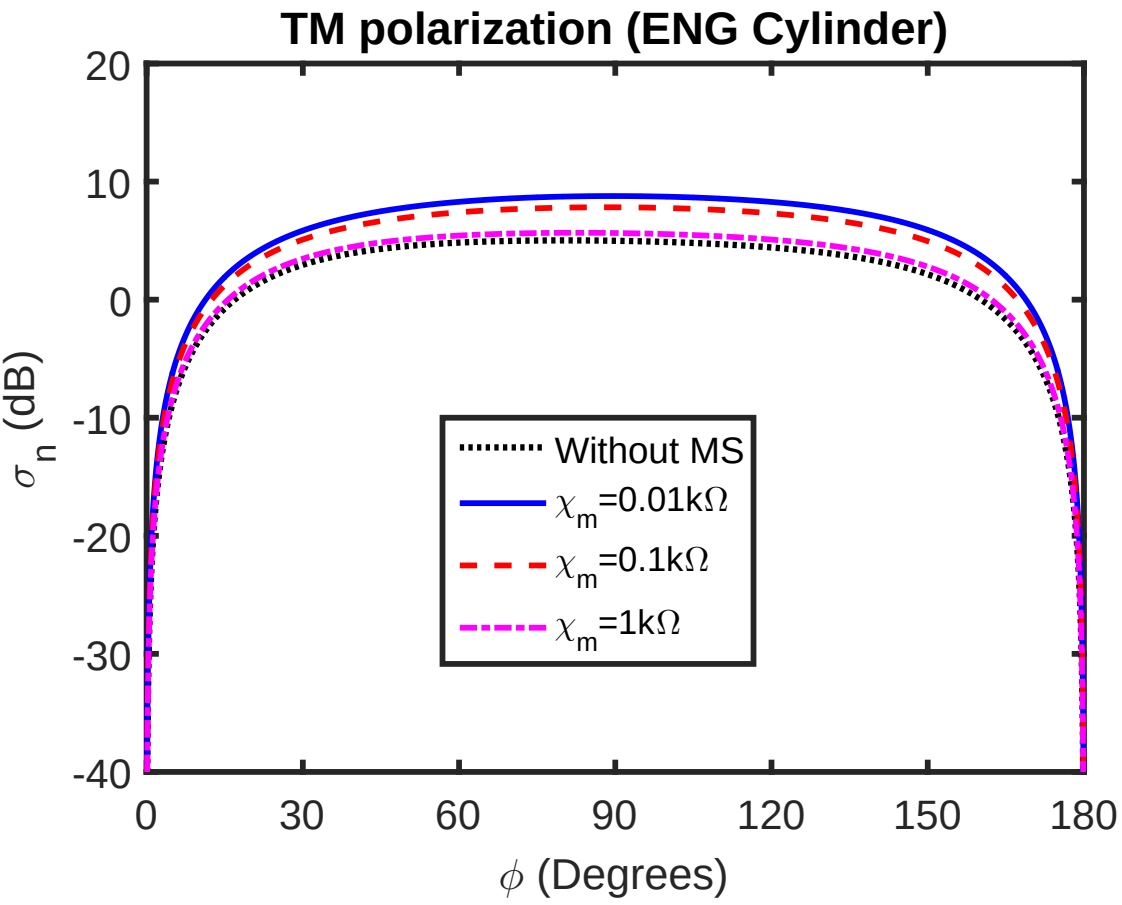

Figure 3.3: Normalized scattering width of an ENG cylinder covered with and without metasurface and buried below a flat interface. Here TM polarization is considered for an ENG cylinder with $\epsilon_r = -2.25$, $\mu_r = 1$. Also we have assumed $\chi_m = 0.01k\Omega$, $0.1k\Omega$ and $1k\Omega$.

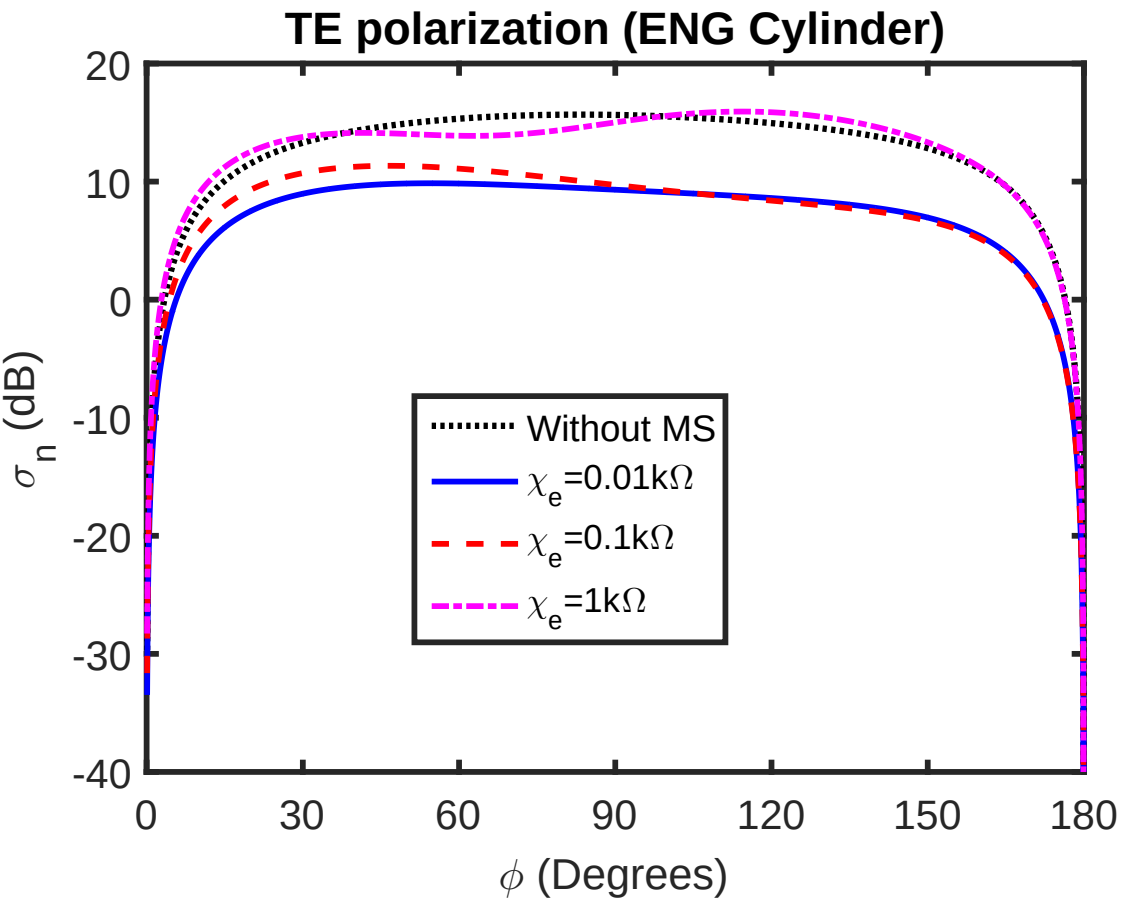

Figure 3.4: Normalized scattering width of an ENG cylinder covered with and without metasurface and buried below a flat interface. Here TE polarization is considered for an ENG cylinder having $\epsilon_r = -2.25$, $\mu_r = 1$ whereas we have assumed $\chi_e = 0.01k\Omega$, $0.1k\Omega$ and $1k\Omega$.

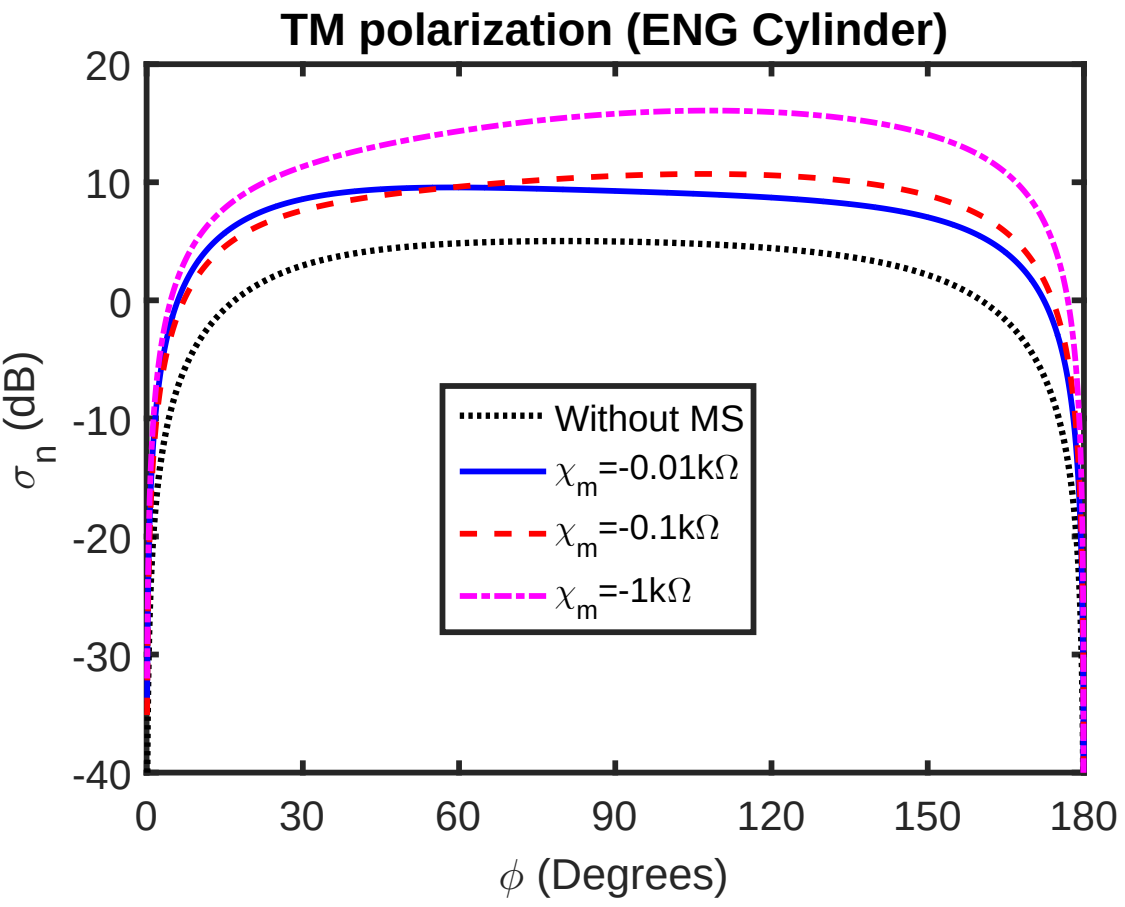

Figure 3.5: Normalized scattering width of an ENG cylinder covered with and without metasurface and buried below a flat interface. Here TM polarization is considered for an ENG cylinder having $\epsilon_r = -2.25$, $\mu_r = 1$. Also it is assumed that $\chi_m = -0.01k\Omega$, $-0.1k\Omega$ and $-1k\Omega$.

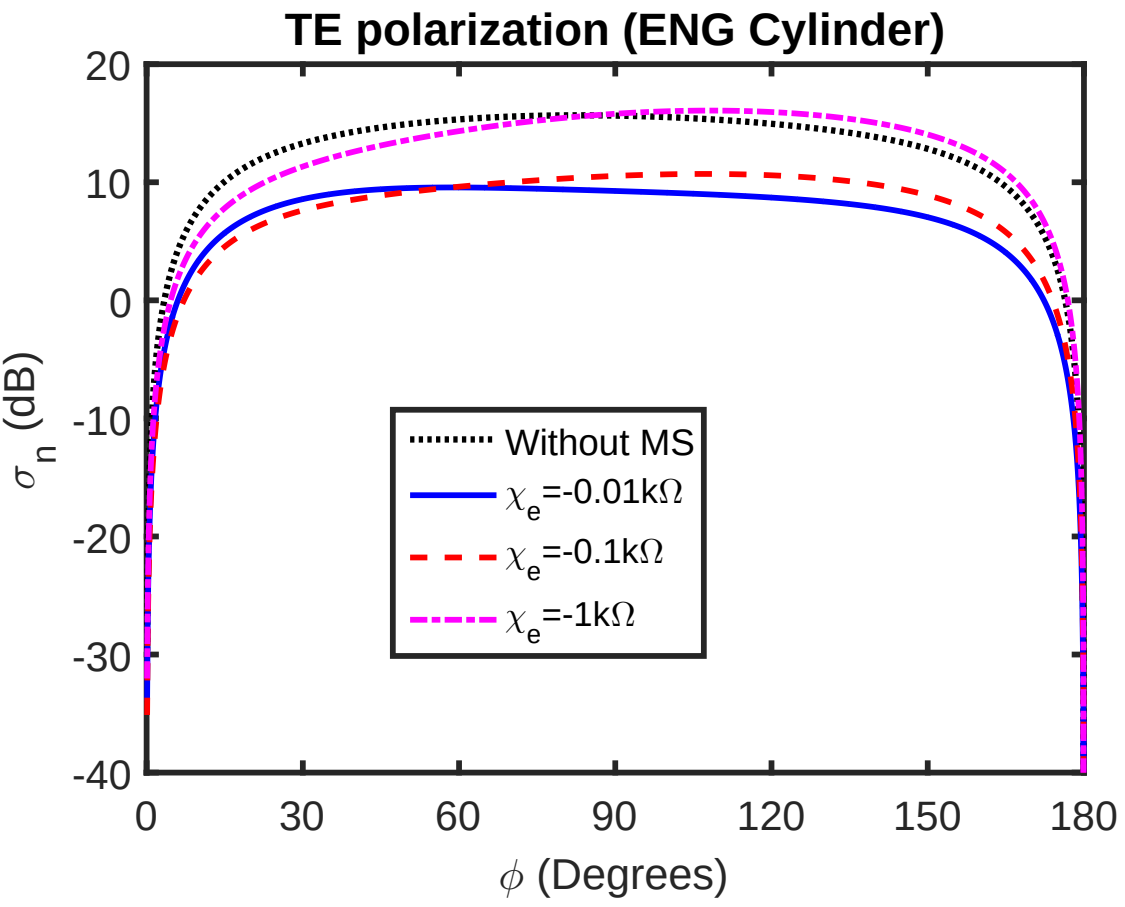

Figure 3.6: Normalized scattering width of an ENG cylinder covered with and without metasurface and buried below a flat interface. Here TE polarization is considered for an ENG cylinder with $\epsilon_r = -2.25$ and $\mu_r = 1$. It is also assumed that $\chi_e = -0.01k\Omega$, $-0.1k\Omega$ and $-1k\Omega$.

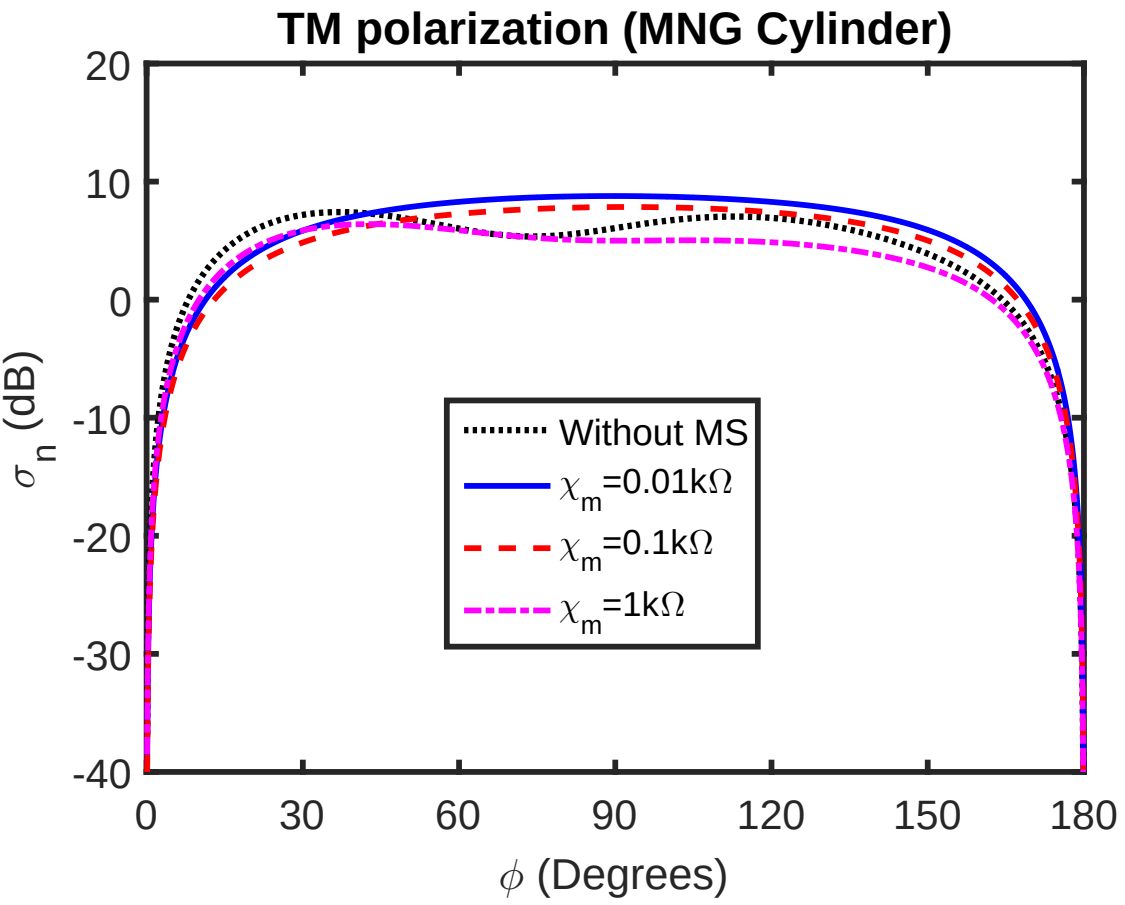

Figure 3.7: Normalized scattering width of an MNG cylinder covered with and without metasurface and buried below a flat interface. Here TM polarization is considered for an MNG cylinder having $\epsilon_r = -1$, $\mu_r = -2.25$. Also it is assumed that $\chi_m = 0.01k\Omega$, $0.1k\Omega$ and $1k\Omega$.

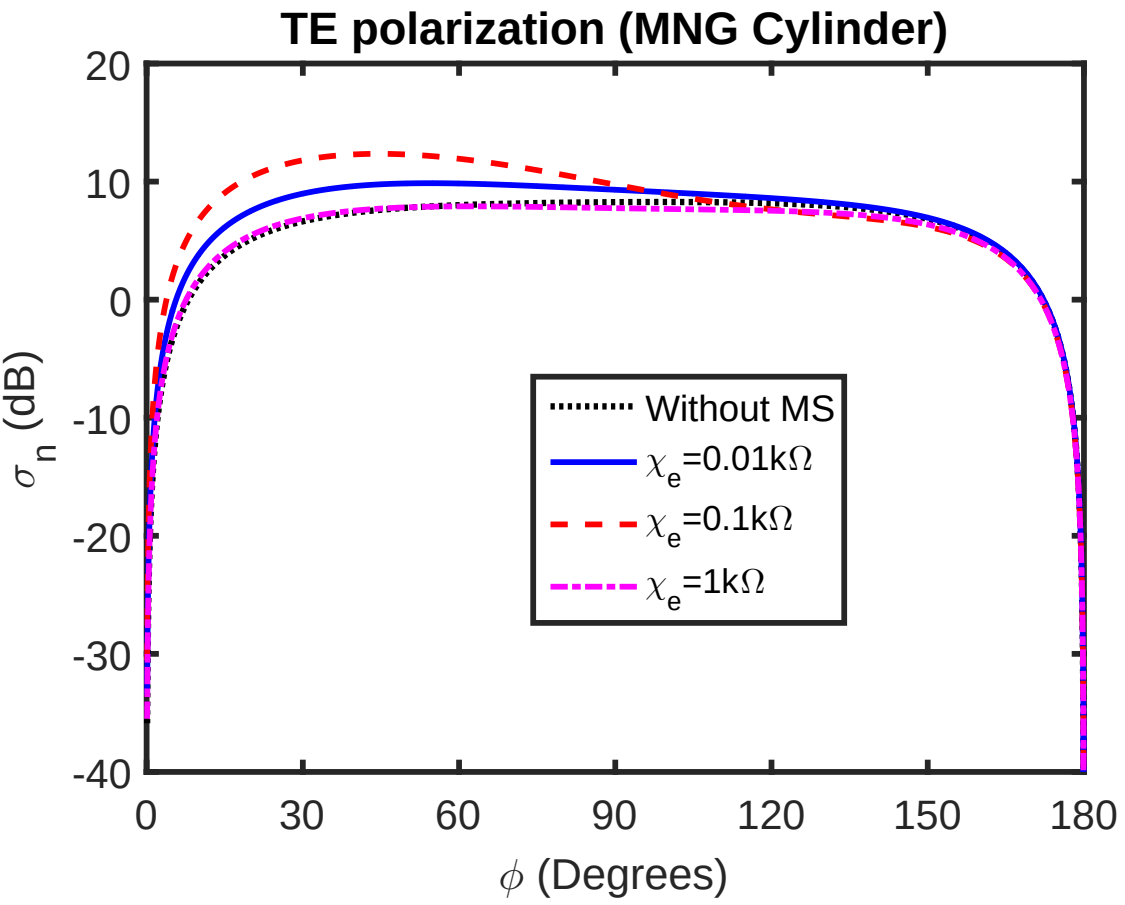

Figure 3.8: Normalized scattering width of an MNG cylinder covered with and without metasurface and buried below a flat interface. Here TE polarization is considered for an MNG cylinder with $\epsilon_r = -1$, $\mu_r = 2.25$. For this case, it is assumed that $\chi_e = 0.01k\Omega$, $0.1k\Omega$ and $1k\Omega$.

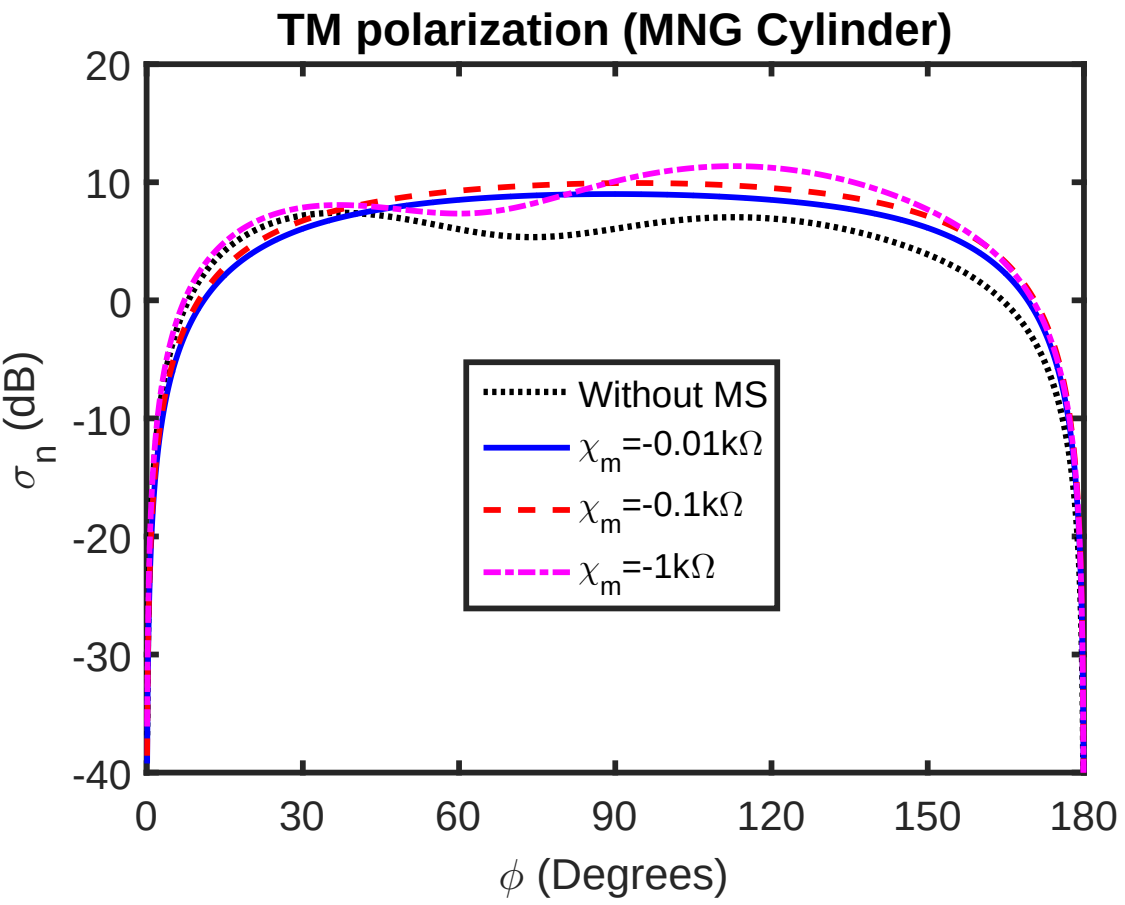

Figure 3.9: Normalized scattering width of an MNG cylinder covered with and without metasurface and buried below a flat interface. Here TM polarization is considered for an MNG cylinder having $\epsilon_r = -1$, $\mu_r = 2.25$. Also we have assumed $\chi_m = -0.01k\Omega$, $-0.1k\Omega$ and $-1k\Omega$.

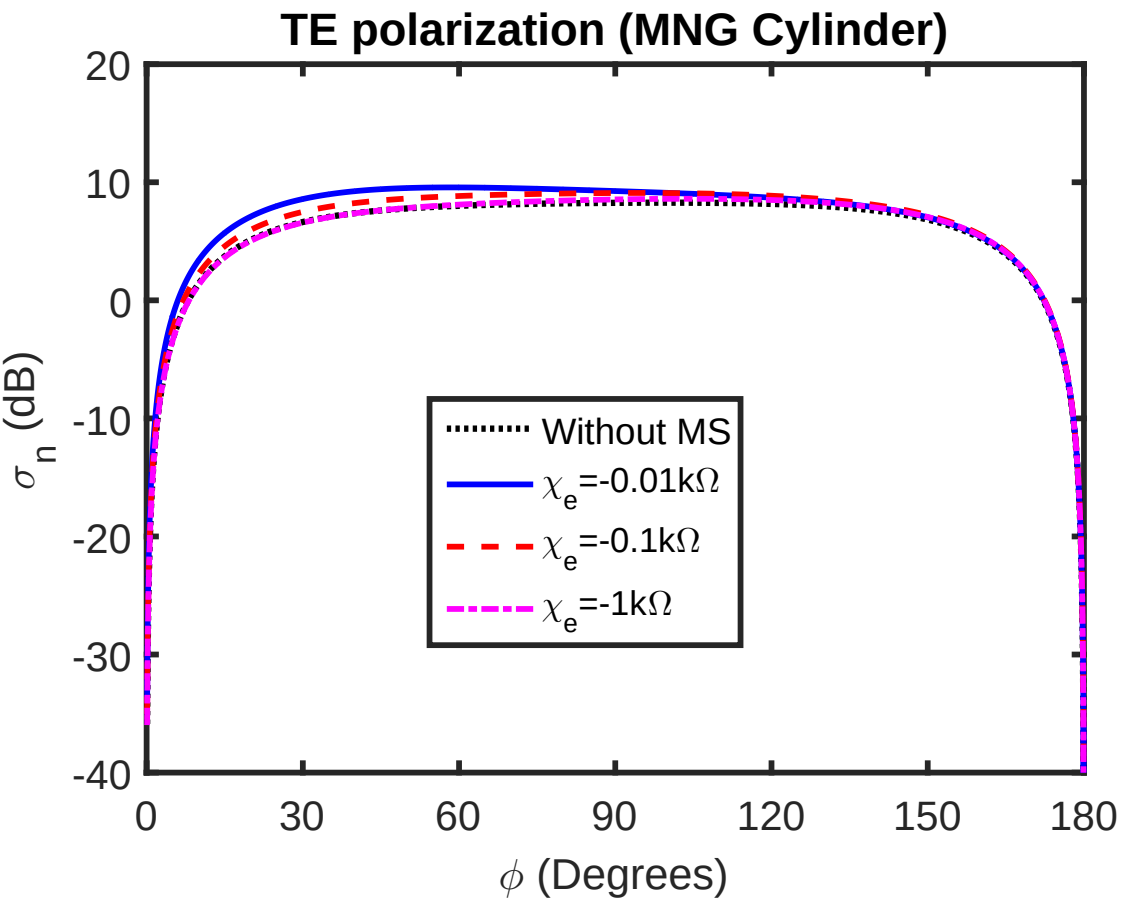

Figure 3.10: Normalized scattering width of an MNG cylinder covered with and without metasurface and buried below a flat interface. Here TE polarization is considered for an MNG cylinder with $\epsilon_r = -1$, $\mu_r = 2.25$. For this case, it is assumed $\chi_e = -0.01k\Omega$, $-0.1k\Omega$ and $-1k\Omega$.

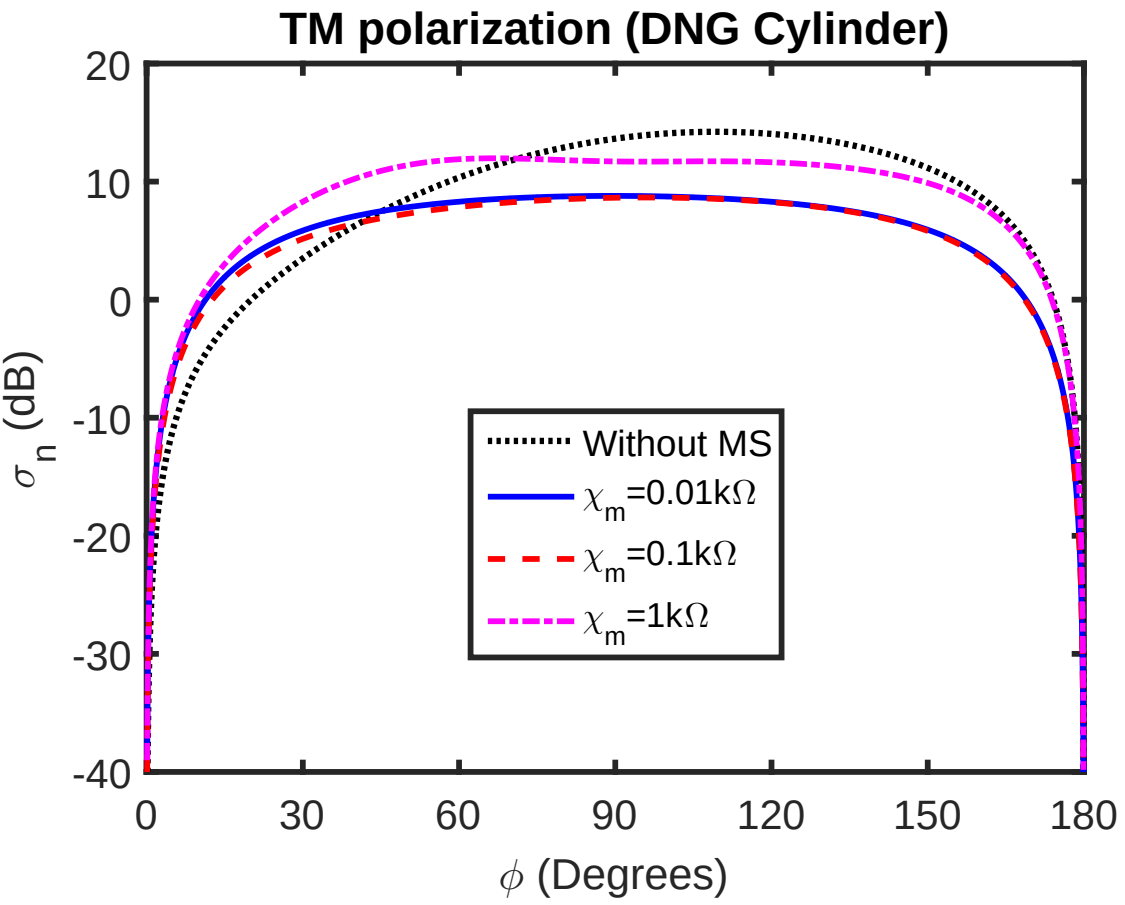

Figure 3.11: Normalized scattering width of an DNG cylinder covered with and without metasurface and buried below a flat interface. Here TM polarization is considered for an DNG cylinder having $\epsilon_r = -2.25$ and $\mu_r = -1$ whereas it is assumed that $\chi_m = 0.01k\Omega$, $0.1k\Omega$ and $1k\Omega$.

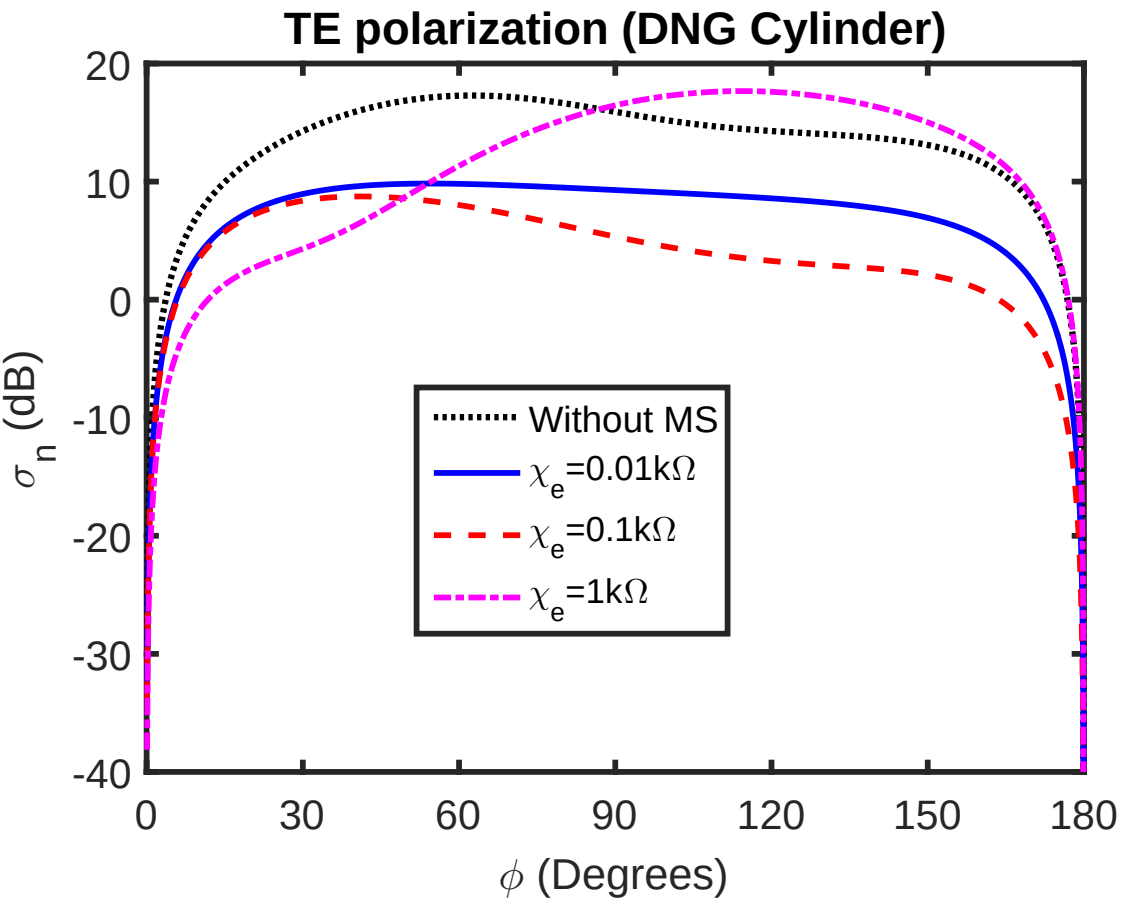

Figure 3.12: Normalized scattering width of an DNG cylinder covered with and without metasurface and buried below a flat interface. Here TE polarization is considered for an DNG cylinder with $\epsilon_r = -2.25$, $\mu_r = -1$. Also we have assumed $\chi_e = 0.01k\Omega$, $0.1k\Omega$ and $1k\Omega$.

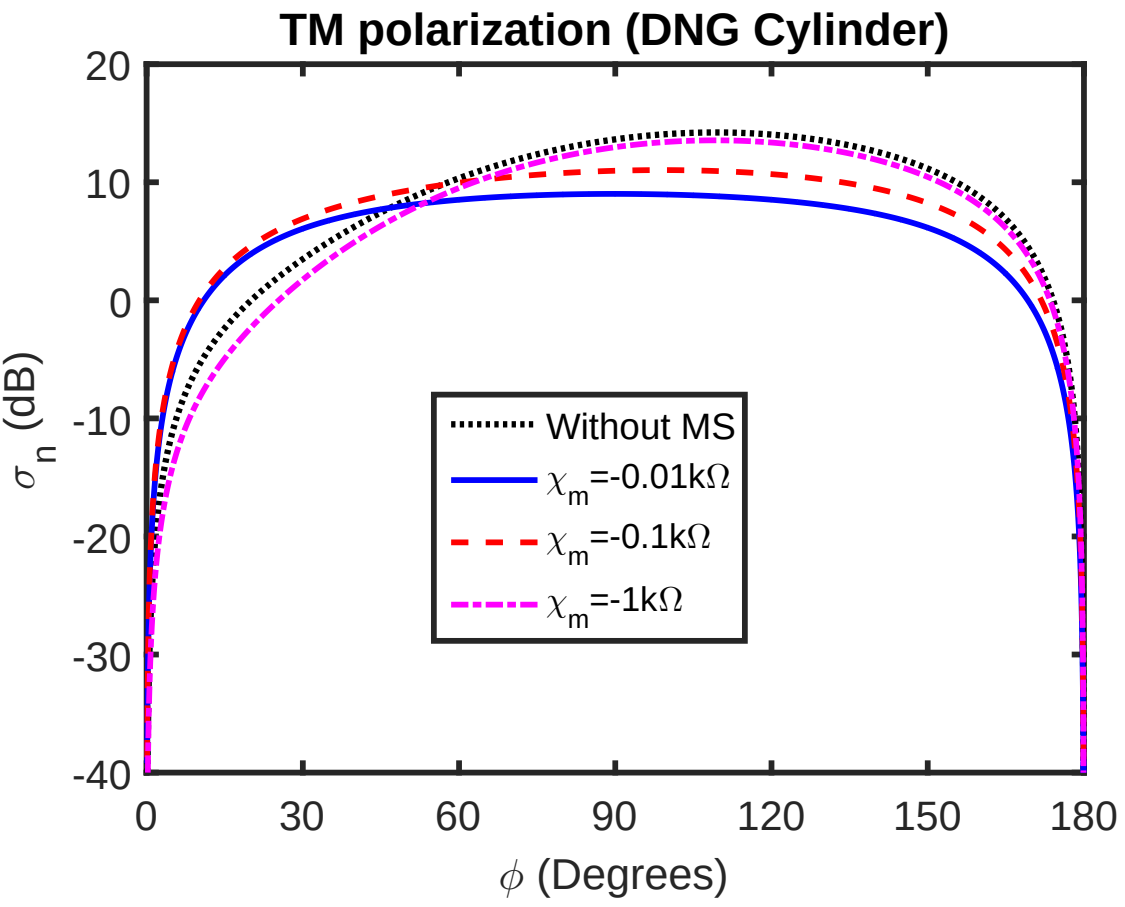

Figure 3.13: Normalized scattering width of an DNG cylinder covered with and without metasurface and buried below a flat interface. Here TM polarization is considered for an DNG cylinder having $\epsilon_r = -2.25$, $\mu_r = -1$. For this case, it is assumed that $\chi_m = -0.01k\Omega$, $-0.1k\Omega$ and $-1k\Omega$.

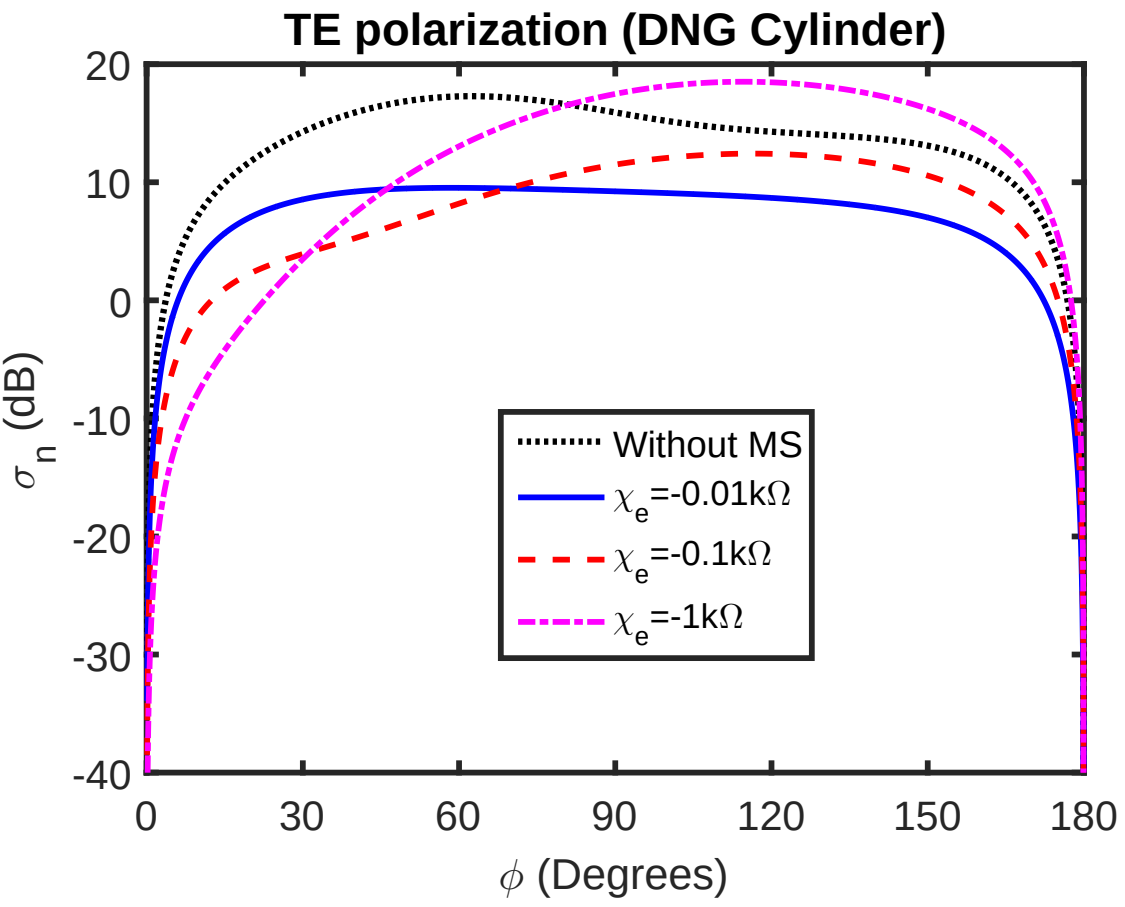

Figure 3.14: Normalized scattering width of an DNG cylinder covered with and without metasurface and buried below a flat interface. Here TE polarization is considered for an DNG cylinder with $\epsilon_r = -2.25$, $\mu_r = -1$. Also we have assumed $\chi_e = -0.01k\Omega$, $-0.1k\Omega$ and $-1k\Omega$.

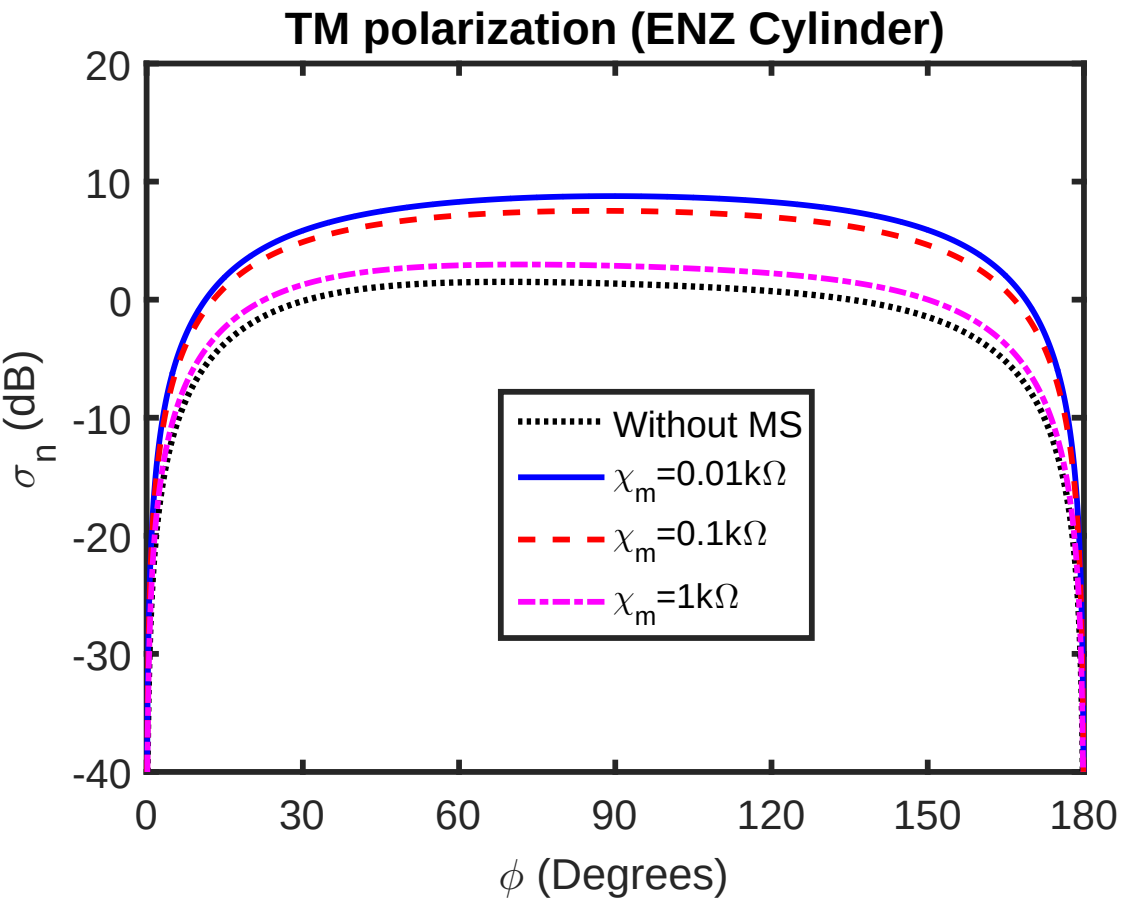

Figure 3.15: Normalized scattering width of an ENZ cylinder covered with and without metasurface and buried below a flat interface. Here TM polarization is considered for an ENZ cylinder having $\epsilon_r = 0.001$, $\mu_r = 1$. For this case, it is assumed that $\chi_m = 0.01k\Omega$, $0.1k\Omega$ and $1k\Omega$.

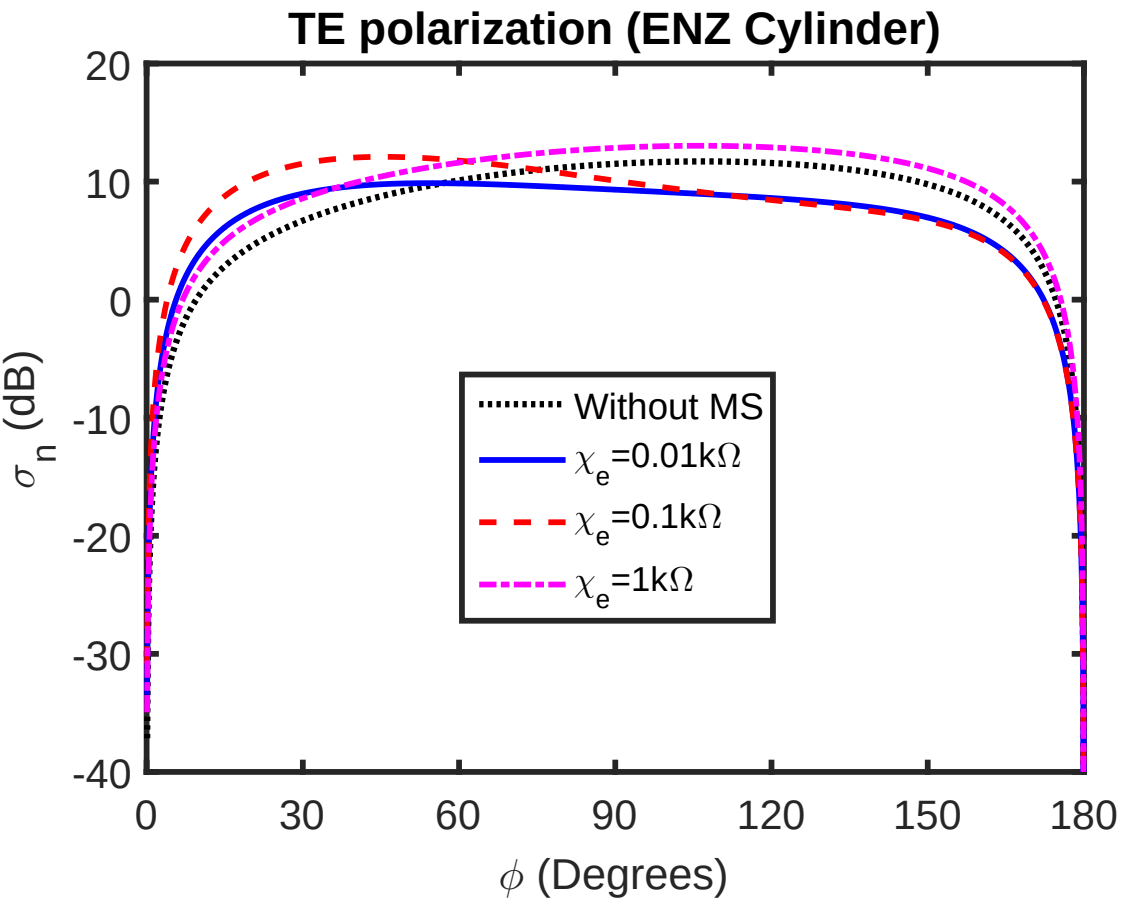

Figure 3.16: Normalized scattering width of an ENZ cylinder covered with and without metasurface and buried below a flat interface. Here TE polarization is considered for an ENZ cylinder with $\epsilon_r = 0.001$, $\mu_r = 1$. It is also assumed that $\chi_e = 0.01k\Omega$, $0.1k\Omega$ and $1k\Omega$.

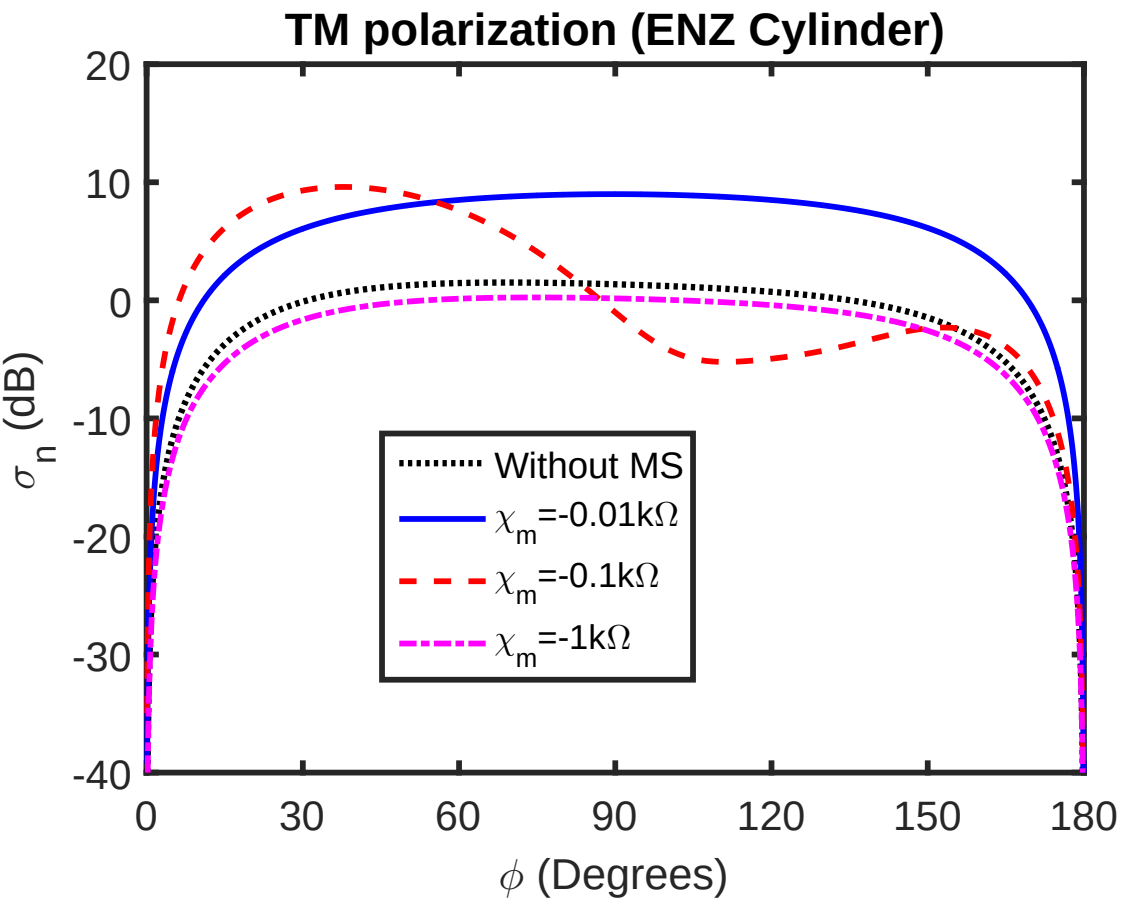

Figure 3.17: Normalized scattering width of an ENZ cylinder covered with and without metasurface and buried below a flat interface. Here TM polarization is considered for an ENZ cylinder having $\epsilon_r = 0.001$, $\mu_r = 1$. Also we have assumed $\chi_m = -0.01k\Omega$, $-0.1k\Omega$ and $-1k\Omega$.

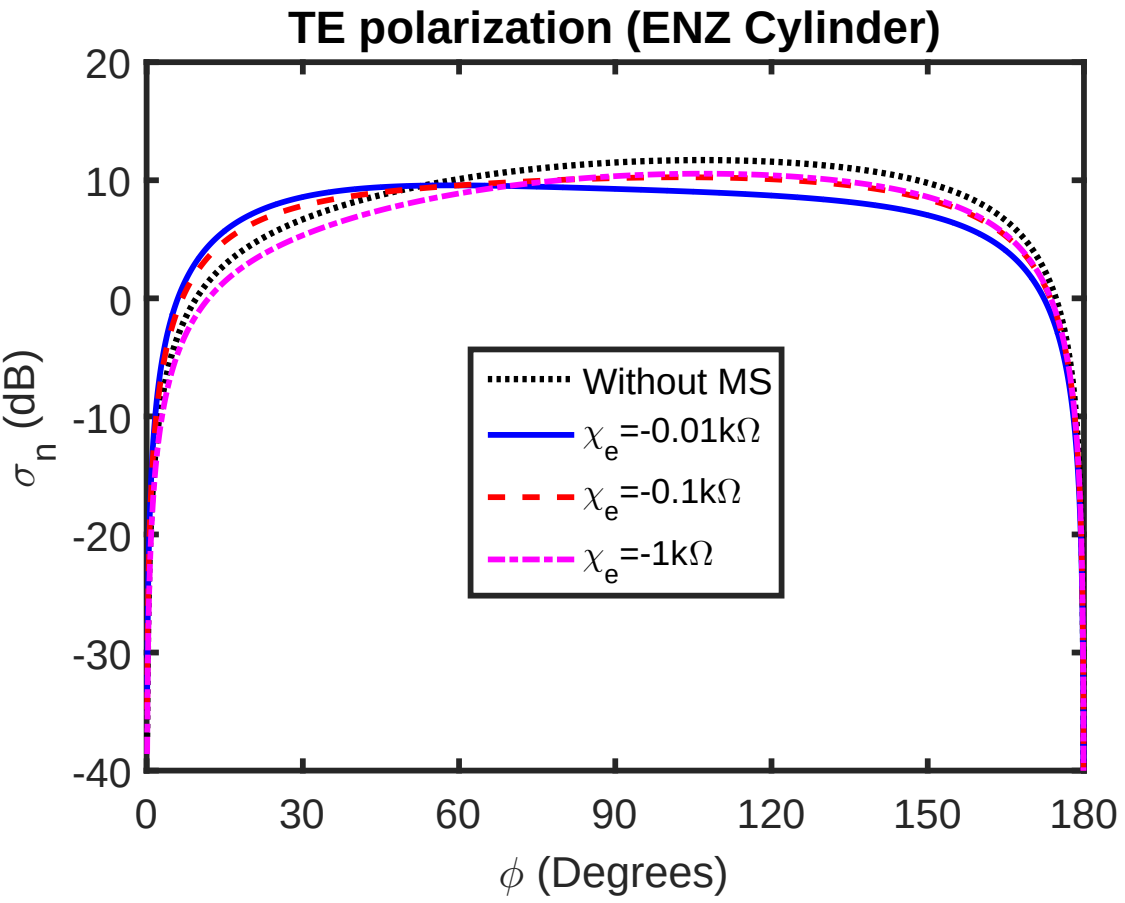

Figure 3.18: Normalized scattering width of an ENZ cylinder covered with and without metasurface and buried below a flat interface. Here TE polarization is considered for an ENZ cylinder with $\epsilon_r = 0.001$, $\mu_r = 1$. For this case, it is assumed that $\chi_m = -0.01k\Omega$, $-0.1k\Omega$ and $-1k\Omega$.

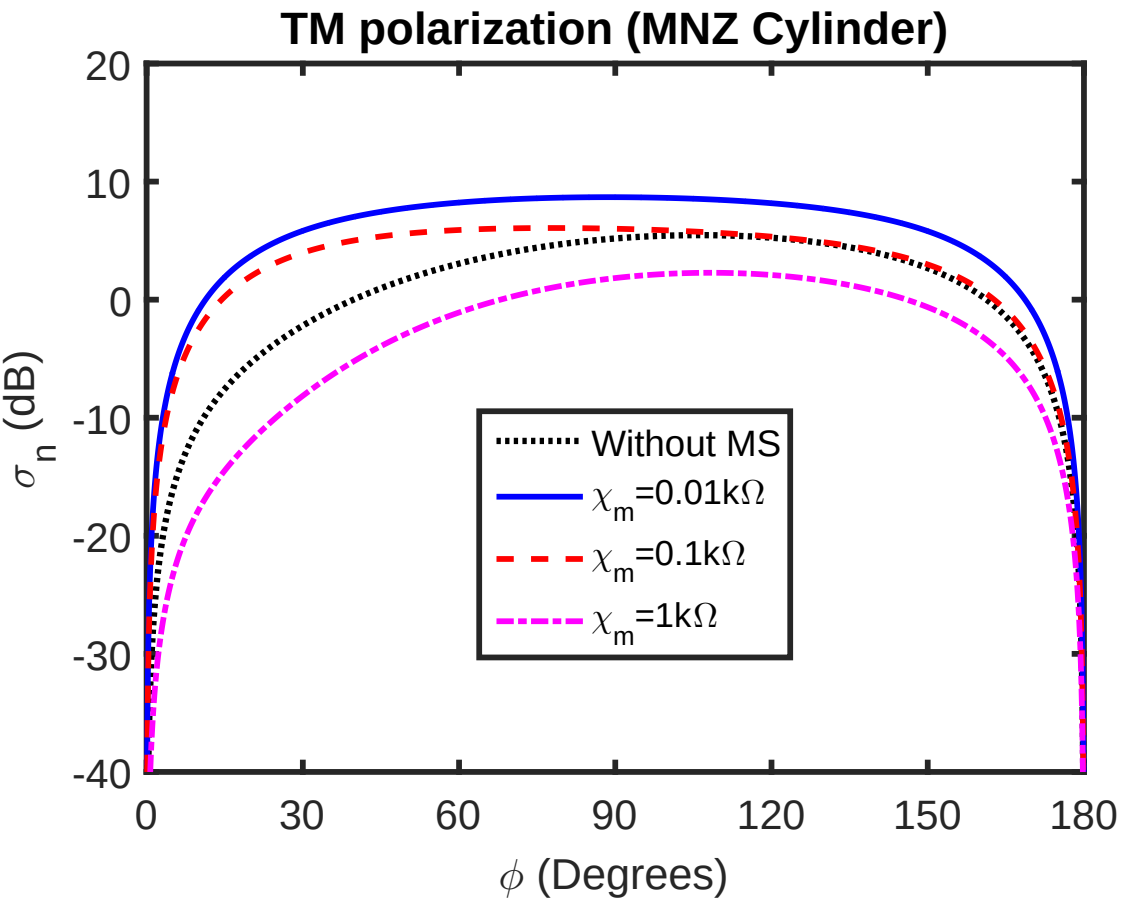

Figure 3.19: Normalized scattering width of an MNZ cylinder covered with and without metasurface and buried below a flat interface. Here TM polarization is considered for an MNZ cylinder having $\epsilon_r = 1$, $\mu_r = 0.001$. Also we have assumed $\chi_m = 0.01k\Omega$, $0.1k\Omega$ and $1k\Omega$.

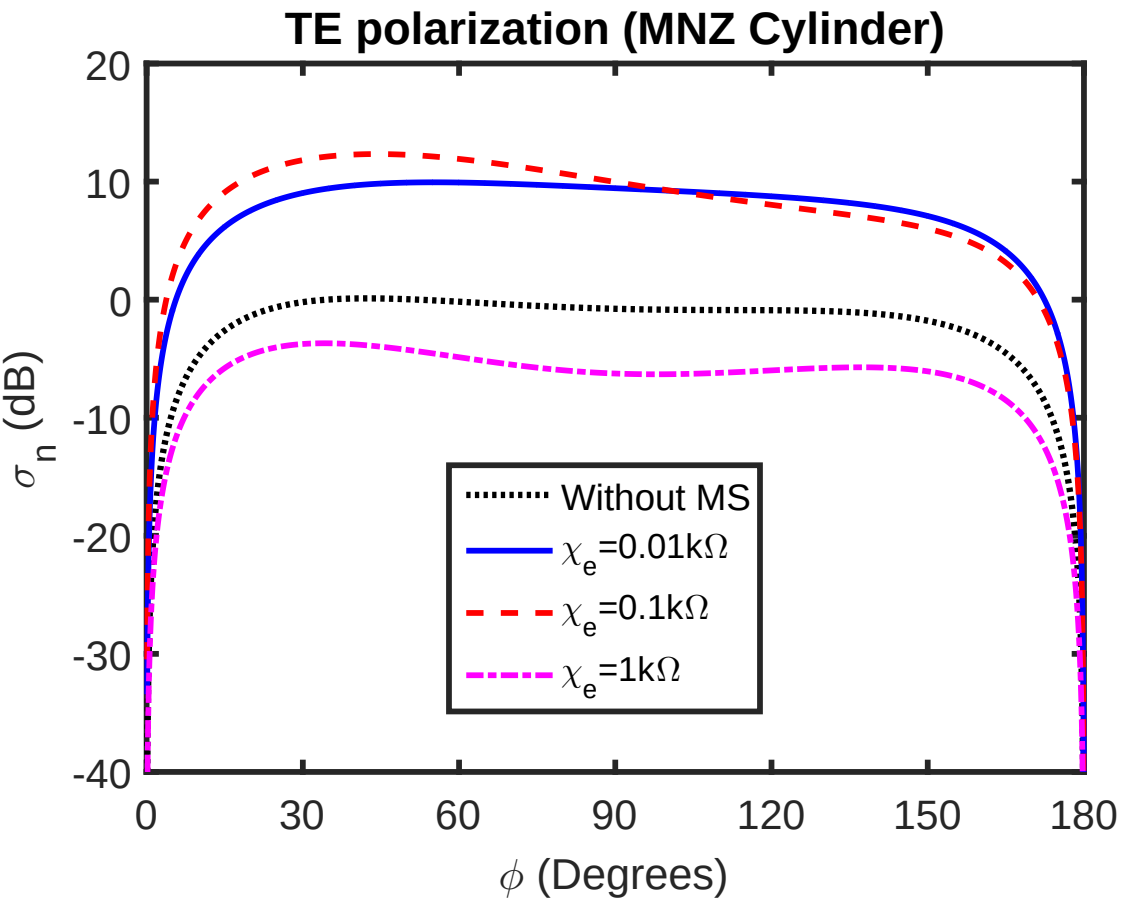

Figure 3.20: Normalized scattering width of an MNZ cylinder covered with and without metasurface and buried below a flat interface. Here TE polarization is considered for an MNZ cylinder with $\epsilon_r = 1$, $\mu_r = 0.001$. For this case, it is assumed that $\chi_e = 0.01k\Omega$, $0.1k\Omega$ and $1k\Omega$.

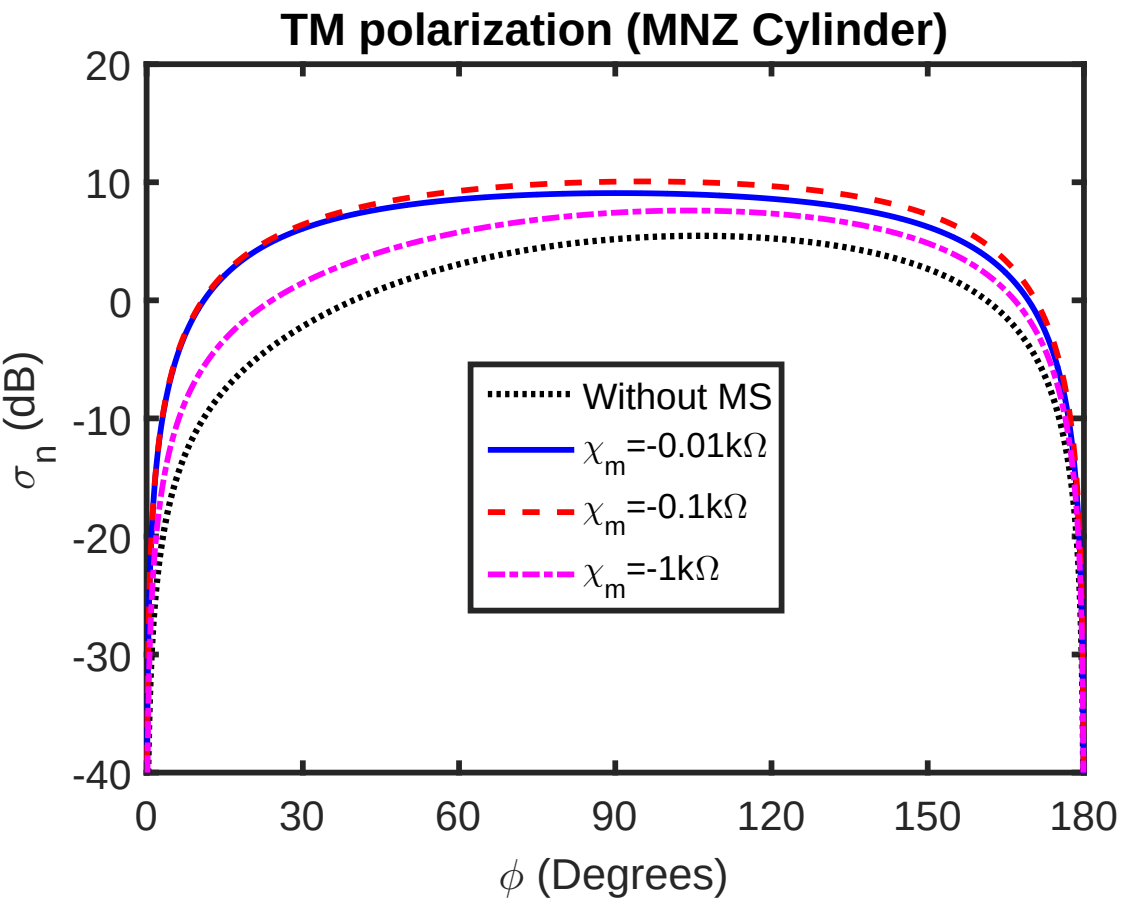

Figure 3.21: Normalized scattering width of an MNZ cylinder covered with and without metasurface and buried below a flat interface. Here TM polarization is considered for an MNZ cylinder having $\epsilon_r = 1$, $\mu_r = 0.001$. Also we have assumed $\chi_m = -0.01k\Omega$, $-0.1k\Omega$ and $-1k\Omega$.

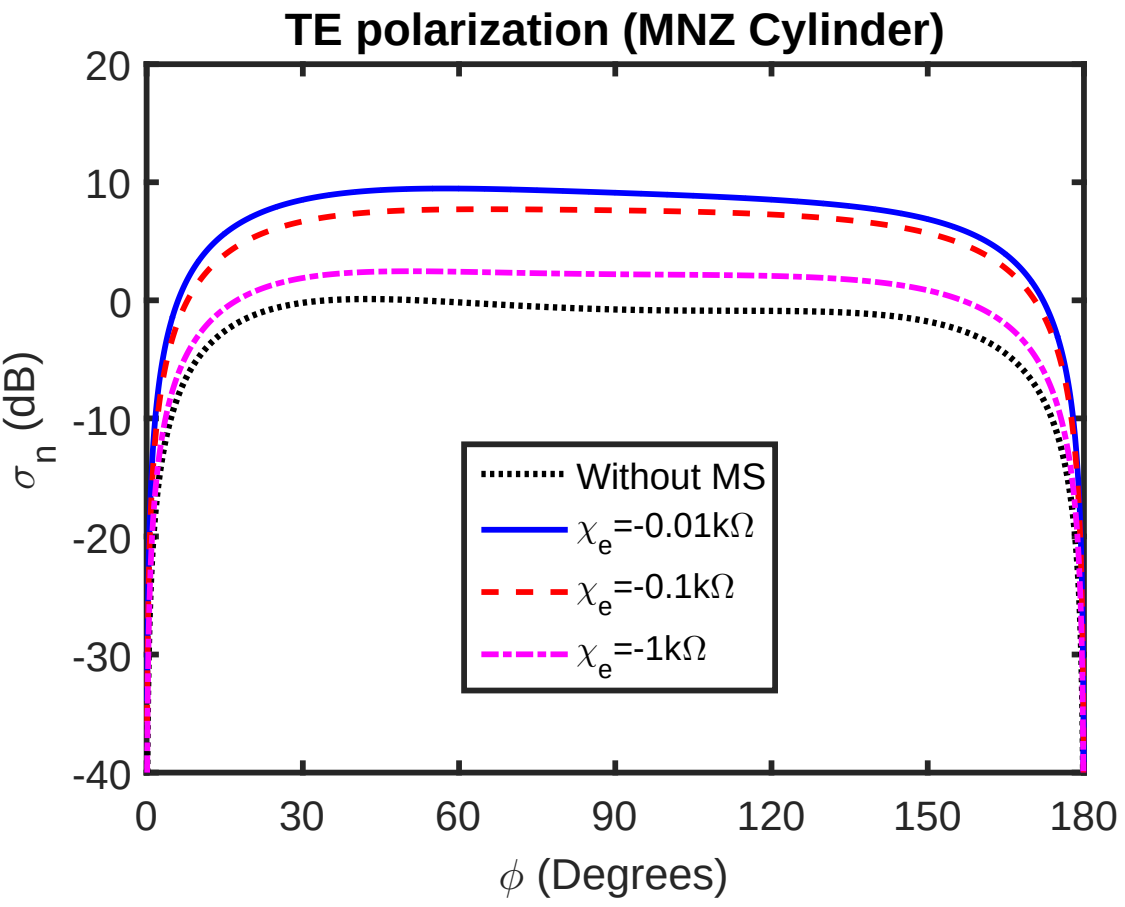

Figure 3.22: Normalized scattering width of an MNZ cylinder covered with and without metasurface and buried below a flat interface. Here TE polarization is considered for an MNZ cylinder with $\epsilon_r = 1$, $\mu_r = 0.001$. It is also assumed that $\chi_e = -0.01k\Omega$, $-0.1k\Omega$ and $-1k\Omega$.

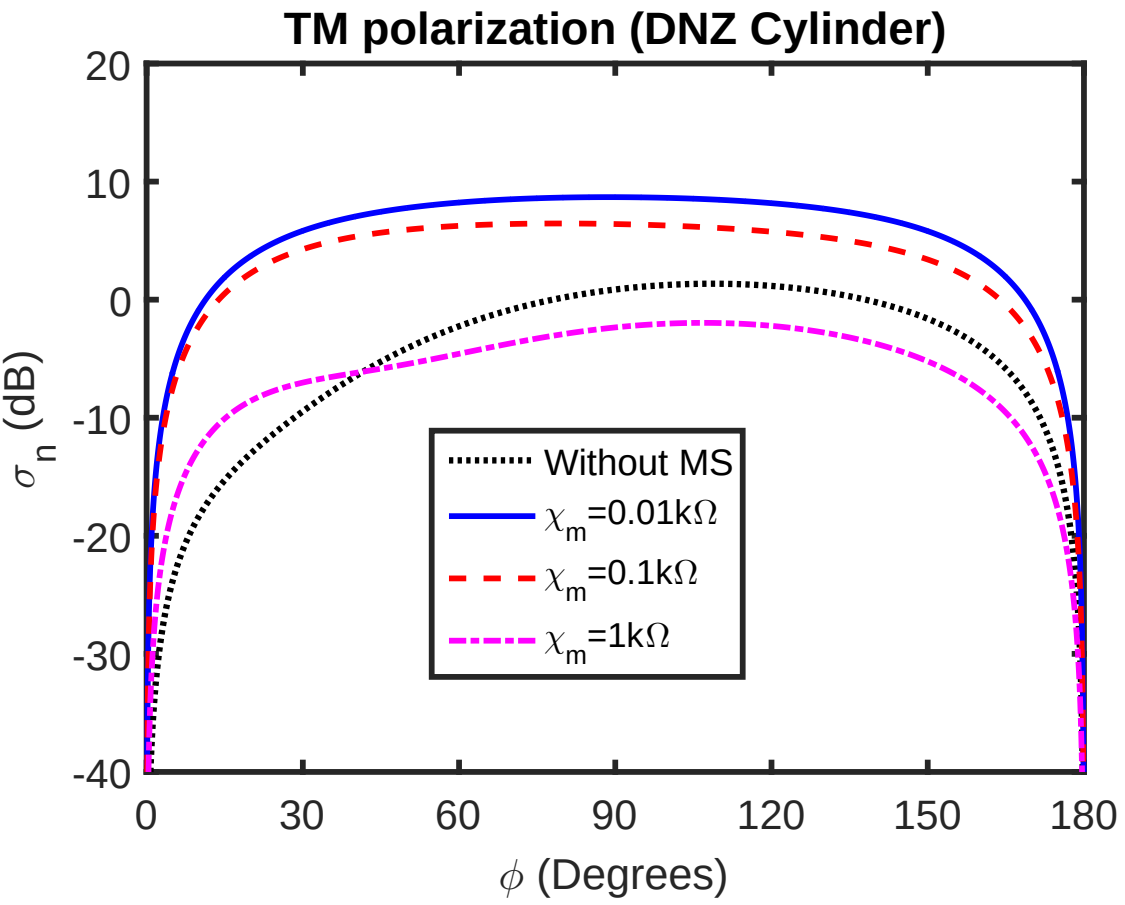

Figure 3.23: Normalized scattering width of an DNZ cylinder covered with and without metasurface and buried below a flat interface. Here TM polarization is considered for an DNZ cylinder having $\epsilon_r = 0.001$, $\mu_r = 0.001$. Also we have assumed $\chi_m = 0.01k\Omega$, $0.1k\Omega$ and $1k\Omega$.

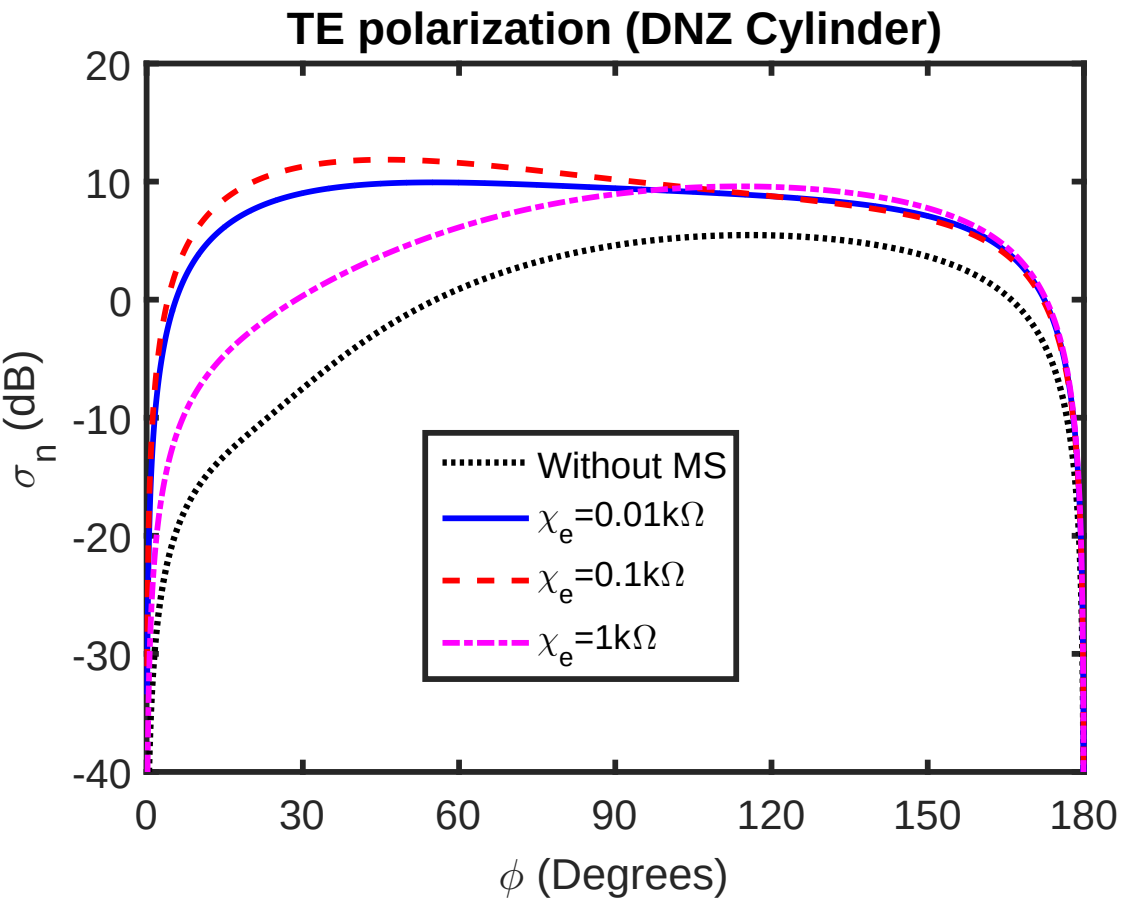

Figure 3.24: Normalized scattering width of an DNZ cylinder covered with and without metasurface and buried below a flat interface. Here TE polarization is considered for an DNZ cylinder with $\epsilon_r = 0.001$, $\mu_r = 0.001$ whereas it is assumed that $\chi_e = 0.01k\Omega$, $0.1k\Omega$ and $1k\Omega$.

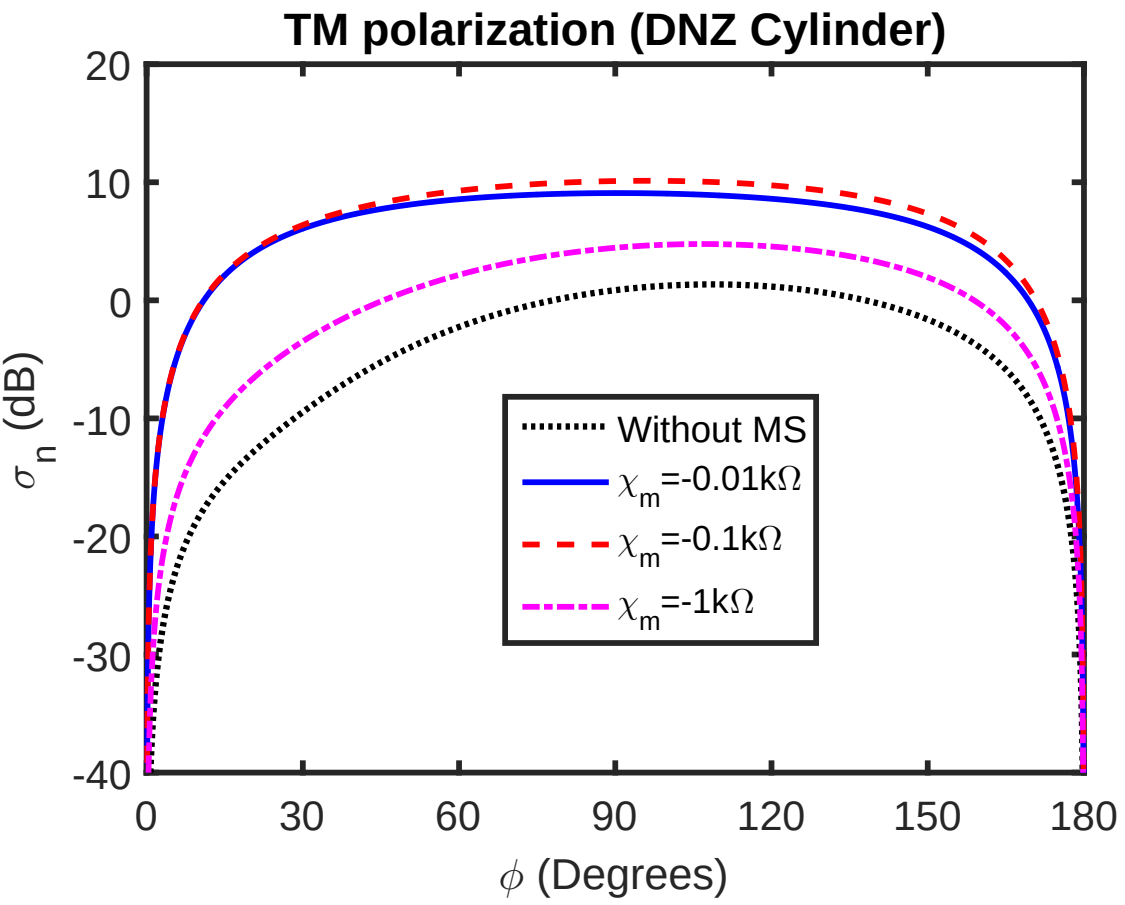

Figure 3.25: Normalized scattering width of an DNZ cylinder covered with and without metasurface and buried below a flat interface. Here TM polarization is considered for an DNZ cylinder with $\epsilon_r = 0.001$, $\mu_r = 0.001$. Also we have assumed $\chi_m = -0.01k\Omega$, $-0.1k\Omega$ and $-1k\Omega$.

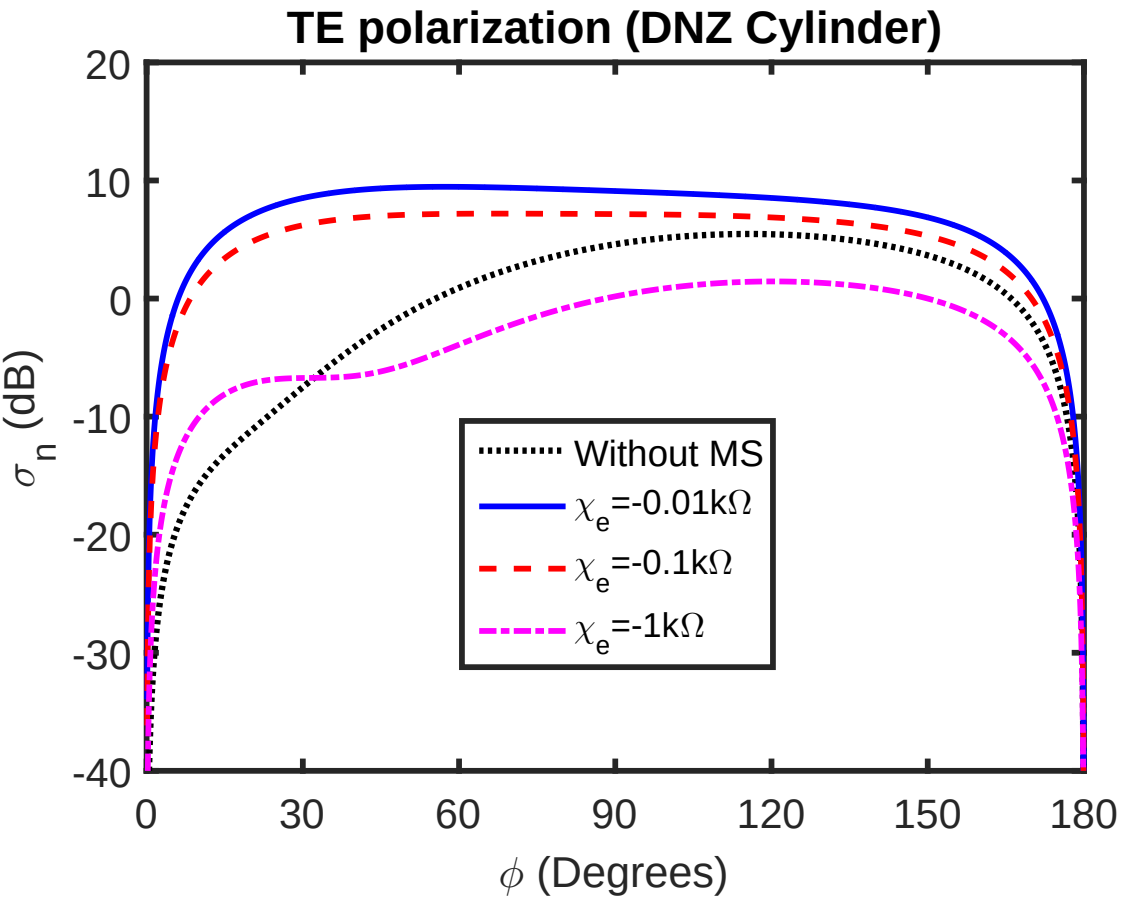

Figure 3.26: Normalized scattering width of an DNZ cylinder covered with and without metasurface and buried below a flat interface. Here TE polarization is considered for an DNZ cylinder having $\epsilon_r = 0.001$, $\mu_r = 0.001$. For this case, it is assumed that $\chi_e = -0.01k\Omega$, $-0.1k\Omega$ and $-1k\Omega$.

Chapter 4

Conclusions and future work

The scattering properties of a metasurface covered metamaterial cylinder buried below a flat interface have been studied. The upper medium of a flat interface is taken to be the free space whereas the lower medium is a dielectric medium. It has been investigated that by varying the permittivity, permeability of the metamaterial cylinder and surface reactances of the metasurface, the scattering width can be enhanced or diminished. This study is helpful in detection of buried metamaterial cylinders with and without metasurface. In future, it is desired to extend the proposed formulation to a metasurface covered multilayered metamaterial cylinder which is buried below a flat interface. Furthermore, the influence of random rough surface and sinusoidal rough surface upon the scattering characteristics of the considered buried cylinders can be investigated.

Bibliography

[1] S. O. Rice, "Reection of electromagnetic waves from slightly rough surfaces," Communications on pure and applied mathematics, Vol. 4, No. 2-3, 351-378, 1951.

[2] D. E. Lawrence and K. Sarabandi, "Acoustic and electromagnetic wave interaction: Analytical formulation for acousto-electromagnetic scattering behavior of a dielectric cylinder," IEEE Trans. Antennas Propagat., Vol. 49, No. 1382–1392, Oct. 2001.

[3] W. R. Jr. Scott, C. T. Schröder and J. S. Martin, "A hybrid acousto/electromagnetic technique for locating land mines," in Proc. Int. Geosci. Remote Sensing Symp., Seattle, 216–218, 1998.

[4] R. Borghi, et al., "Plane-wave scattering by a perfectly conducting circular cylinder near a plane surface: cylindrical-wave approach," JOSA A, Vol. 13, No. 3, 483493, 1996.

[5] B. P. D'Yakonov, "The diffraction of electromagnetic waves by a circular cylinder in a homogeneous half space," Bull. Acad. Sci. No., 950-–955, 1959.

[6] S. O. Ogunade, "Electromagnetic response of an embedded cylinder for line current excitation," Geophysics, Vol. 46, No. 1, 45-–52, 1981.

[7] N. V. Budko, and P. M. van den Berg, "Characterization of a two-dimensional subsurface object with an eective scattering model," IEEE Transactions on Geoscience and Remote Sensing," Vol. 37, No. 5, 2585–2596, 1999.

[8] C. Butler, X. B. Xu, and A. Glisson. "Current induced on a conducting cylinder located near the planar interface between two semi-innite half-spaces," IEEE Transactions on Antennas and Propagation, Vol. 33, No. 6, 616–624, 1985.

[9] X. B. Xu and C. Butler, "Current induced by TE excitation on a conducting cylinder located near the planar interface between two semi-innite half-spaces," IEEE Transactions on Antennas and Propagation, Vol. 34, No. 7, 880–890, 1986.

[10] G. Zhang, L. Tsang and K. Pak, "Angular correlation function and scattering coefficient of electromagnetic waves scattered by a buried object under a two-dimensional rough surface," JOSA A, Vol. 15 No. 12, 2995–3002, 1998

[11] M. El-Shenawee and C. Rappaport, "Monte Carlo simulations for clutter statistic in mineelds: AP-mine-like-target buried near a dielectric object," IEEE Trans. Geosci. Remote Sensing, Vol. 40, 1416–1426, 2002.

[12] G. A. Ellis and I. C. Peden, "An analysis technique for buried inhomogeneous dielectric object in the presence of an air-earth interface," IEEE Trans. Geosci. Remote Sens., Vol. 33, 535-–540, 1995.

[13] C. M. Butler and X. B. Xu, "Scattering by a lossy dielectric cylinder buried below the planar interface between two semi-infinite half spaces," paper presented at 1989 Radio Science Meeting, Union Radio Sci. Int., San Jose, Calif., June 1989.

[14] X.-B. Xu and J. Ao, "A hybrid integral and differential equation method solution of scattering of TM excitation by buried inhomogeneous cylinders," Progress in Electromagnetics Research, No. 15, 165—189, 1997.

[15] A. Alu and N. Engheta, "Pairing an elipson-negative slab with a mu-negative slab: resonance, tunneling and transparency," IEEE Trans. Antennas and propagation, Vol. 51, 2558–2571, 2003.

[16] A. Alu and N. Engheta, "Guided modes in a waveguide filled with a pair of single-negative (SNG), double negative (DNG), and/or double-positive (DPS) layers," IEEE Trans. Microwave Theory and Techniques, Vol. 52, 199–210, 2004.

[17] N. Engheta, A. Alu, M. G Silveirinha, A. Salandrino and J. Li, "DNG, SNG, ENZ and MNZ metamaterials and their potential applications," IEEE MELECON 16-19, Benalmadena, Spain, 2006.

[18] A. Alu and N. Engheta, "Polarizabilities and effective parameters ofcollections of spherical nanoparticles formed by pairs of concentric double-negative (DNG), single negative (SNG) shells, and/or double-positive (DPS) metamaterial layers," Journal of Applied Physics, Vol. 97, 094310, 2005.

[19] S. Maci, G. Minatti, M. Casaletti, and M. Bosiljevac, "Metasurfing: Addressing waves on impenetrable metasurfaces," IEEE Antennas and Wireless Propagation Letters, Vol. 10, 1499–1502, 2011.

[20] C. L. Holloway, E. F. Kuester, J. A. Gordon, J. O'Hara, J. Booth, and D. R. Smith, "An overview of the theory and applications of metasurfaces: The two-dimensional

equivalents of metamaterials," IEEE Antennas and Propagation Magazine, Vol. 54, No. 2, 10–35, 2012.

[21] S. Maci, A. Cucini, N. Engheta, and R. W. Ziolkowski, "FSS-based complex surfaces," in Electromagnetic Metamaterials: Physics and Engineering Aspects, Eds. NJ: Wiley, 2006.

[22] O. Luukkonen, C. Simovski, G. Granet, G. Goussetis, D. Lioubtchenko, A. V. Raisanen, S. A. Tretyakor, "Simple and accurate analytical model of planar grids and high-impedance surfaces comprising metal strips or patches," IEEE Transactions on Antennas and Propagation, Vol. 56, No. 6, 1624–1632, 2008.

[23] D. Ramaccia, A. Toscano, and F. Bilotti, "A new accurate model of high-impedance surfaces consisting of circular patches," Progress in Electromagnetics Research M, Vol. 21, 1–17, 2011.

[24] H. J. Bilow, "Guided waves on a planar tensor impedance surface," IEEE Transactions on Antennas and Propagation, Vol. 51, No. 10, 2788–2792, 2003.

[25] A. M. Patel and A. Grbic, "The effects of spatial dispersion on power flow along a printed-circuit tensor impedance surface," IEEE Transactions on Antennas and Propagation, Vol. 62, No. 3, 1464–1469, 2014.

[26] E. Martini and S. Maci, "Metasurface transformation theory Transformation Electromagnetics and Metamaterials," D. H. Werner and D. H. Kwon, Eds. London: Springer, 2014.

[27] A. M. Patel and A. Grbic, "Transformation electromagnetics devices using tensor impedance surfaces," In 2013 IEEE MTT-S International Microwave Symposium Digest (MTT), 1–4, June 2, 2013.

[28] M. Mencagli, E. Martini and S. Maci, "Surface wave dispersion for anisotropic metasurfaces constituted by elliptical patches," IEEE Transactions on Antennas and Propagation, Vol. 63, No. 7, 2992–3003, 2015.